. SCUOLA INTERNAZIONALE SUPERIORE DI STUDI AVANZATI

SISSA Digital Library

Reduced Basis Approaches in Time-Dependent Non-Coercive Settings for Modelling the Movement of Nuclear Reactor Control Rods

Original

Availability:
This version is available at: 20.500.11767/15968 since:

Publisher:

Published
DOI:10.4208/cicp.120914.021115a

Terms of use:

Testo definito dall'ateneo relativo alle clausole di concessione d'uso

Publisher copyright

note finali coverpage

(Article begins on next page)

08 September 2026

Reduced basis approaches in time-dependent non-coercive settings for modelling the movement of nuclear reactor control rods

Alberto Sartori[1,2], Antonio Cammi[1], Lelio Luzzi[1], and Gianluigi Rozza[2,*]

[1] *Politecnico di Milano - Department of Energy,*
CeSNEF, Enrico Fermi Center for Nuclear Studies,
via La Masa 34, 20156 Milano (Italy)
[2] *SISSA, International School for Advanced Studies, Mathematics Area - mathLab,*
Via Bonomea 265, 34136 Trieste (Italy)

Abstract. In this work, two approaches, based on the certified Reduced Basis method, have been developed for simulating the movement of nuclear reactor control rods, in time-dependent non-coercive settings featuring a 3D geometrical framework. In particular, in a first approach, a piece-wise affine transformation based on subdomains division has been implemented for modelling the movement of one control rod. In the second approach, a "staircase" strategy has been adopted for simulating the movement of all the three rods featured by the nuclear reactor chosen as case study. The neutron kinetics has been modelled according to the so-called multi-group neutron diffusion, which, in the present case, is a set of ten coupled parametrized parabolic equations (two energy groups for the neutron flux, and eight for the precursors). Both the reduced order models, developed according to the two approaches, provided a very good accuracy compared with high-fidelity results, assumed as "truth" solutions. At the same time, the computational speed-up in the Online phase, with respect to the fine "truth" finite element discretization, achievable by both the proposed approaches is at least of three orders of magnitude, allowing a real-time simulation of the rod movement and control.

Key words: reduced basis method, control rod movement, spatial kinetics, parametrized geometry, multi-group neutron diffusion, non-coercive operators.

1 Introduction

In the development of the control systems, the preliminary stage of modelling mainly concerns the correct evaluation of the representative system time constants, and getting

*Corresponding author. *Email addresses:* alberto.sartori@polimi.it (A. Sartori), antonio.cammi@polimi.it (A. Cammi), lelio.luzzi@polimi.it (L. Luzzi), gianluigi.rozza@sissa.it (G. Rozza)

the fundamental aspects related to the system response to the outside perturbations. In the analysis of the whole nuclear reactor kinetics, which is governed by the neutronics, the most spread approach is constituted by the *point-kinetics* equations [34]. This description of the neutronics is based on a set of coupled non-linear ordinary differential equations that describe both the time-dependency of the neutron population in the reactor and the decay of the delayed neutron precursors, allowing for the main feedback reactivity effects. Among the several assumptions entered in the derivation of these equations, the strongest approximation regards the shape of the neutron flux, which is assumed to be represented by a single, time-independent spatial mode [34].

Nuclear reactors are generally characterised by complex geometries and may feature asymmetric core configurations. Therefore, more accurate and complex modelling approaches might be needed to provide more detailed insights concerning the reactor behaviour during operational transients. It is worth mentioning that innovative reactor concepts, for instance Generation IV reactors [9], feature power density and temperature ranges, experienced by structural materials, such that the corresponding spatial dependency cannot be neglected. Moreover, in order to develop suitable control strategies for such reactors, the spatial effects induced by the movement of the control rods have to be taken into account as well.

In this context, a computational reduced order technique, such as the Reduced Basis (RB) method [27,30], can lead to a simulation tool with real-time simulation, still solving a set of partial differential equations. The goal of a computational reduction technique [23] is to capture the essential features of the input/output behaviour of a system in a rapid, accurate and reliable way, i.e. (i) by improving computational performances and (ii) by keeping the approximation error between the reduced-order solution and the full-order solution under control. In particular, it aims at approximating a parametrized partial differential equation (or a set of partial differential equations) solution with a handful of degrees of freedom instead of thousands or millions that would be needed for a full-order approximation. In this way, the full-order problem has to be solved for a suitable number of instances of the input parameter (through a very demanding Offline computational step), in order to be able to perform many low-cost real-time simulations (inexpensive Online computational step) for several new instances of the parameter.

In the present work, the Reduced Basis method (built upon a high-fidelity "truth" Finite Element (FE) approximation, relying on the `libMesh` library [15]) has been applied to model real-time control rod movement within a nuclear reactor, based on the neutron diffusion coupled equations, simulating a 3D framework, with reference to the TRIGA Mark II nuclear reactor [7] of the University of Pavia (Italy). In particular, two different parametrized models have been considered: a first one, with just one rod, then a second one with three control rods. The physics has been modelled by time-dependent non-coercive parametrized equations. Indeed, the neutron kinetics has been described by means of parametrized multi-group time-dependent diffusion equations [5], which are a set (ten in the present work) of coupled parabolic equations where the heights of the control rods (i.e., how much the rods are inserted) play the role of the varying parameters.

For the one-rod model, a piecewise affine transformation based on subdomain division has been implemented [30]. On the other hand, for the three-rods model, the movement of the control rods has been discretized by splitting the rods in many subdomains, which are like "steps".

This contribution stems from the need of nuclear engineering field to have a fast-running simulation tool, which can be tailored to common control systems, able to reproduce spatial effects [31], in particular those induced by the control rod movement, in order to build a bridge between the "world of design" and the "world of control". The goal is to demonstrate that reduced order modelling is suited to be applied in more complex (and coupled) industrial problems in order to introduce competitive computational performances and allowing, at the same time, a better investigation towards more complex industrial problems, thanks to parametrization of involved phenomena. The original elements introduced in this work are related to reduced order modelling approaches in a complex parametrized industrial systems modelled into a 3D geometrical setting, which is held by a system of several time-dependent non-coercive coupled equations whose solutions have been verified by accurate error bounds. At the best of our knowledge and at the current state of the art this is the first time that the certified reduced basis method has been employed to these problems.

The paper is organised as follows. The TRIGA Mark II reactor and the so called neutron diffusion equations are briefly introduced in Section 2. Thereafter, the Reduced Basis method, which is detailed in Section 3, is applied to the parametrized reactor spatial kinetics for the one-rod model (Section 4) and for the three-rods model (Section 5), highlighting some representative results. Conclusions and future perspectives are presented in Section 6. Finally, for the sake of completeness, a simple worked problem to illustrate how to compute the coefficients of the piece-wise affine transformation is detailed in Appendix A.

2 Fundamentals of nuclear reactors modelling

In the following, the TRIGA Mark II reactor and the neutron kinetics are briefly introduced as fundamental element and phenomenon in the parametrized system.

2.1 The TRIGA Mark II reactor

As anticipated, the TRIGA Mark II reactor [7] of the University of Pavia (Italy) has been chosen as case study. Such system is a pool-type reactor whose core features a non-symmetric configuration, beside being cooled with water in natural convection. Figure 1 shows the map of the core, which features three control rods (SHIM, TRANS, REG), two irradiation channels (C.T., RABBIT), and one channel where the source for the start-up of the reactor is placed surrounded by two elements of graphite (DUMMY). All other elements are fuel pins. It is worth recalling that this work is more focused on testing and

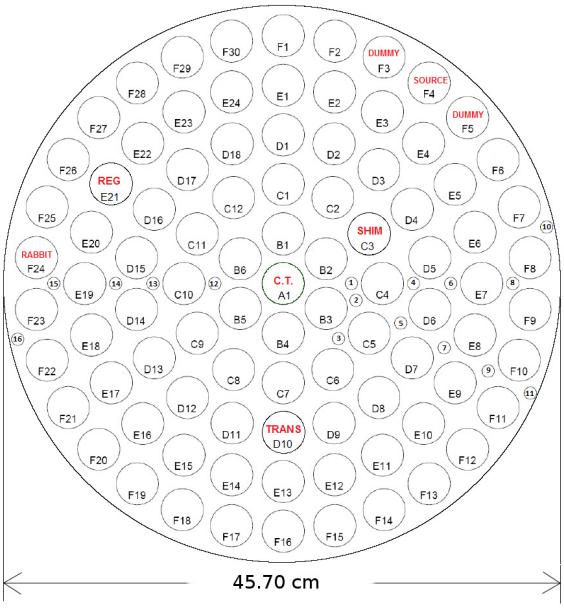

Figure 1: Map of the TRIGA Mark II reactor core.

assessing an innovative methodology for a 3D reactor spatial dynamics, rather than reproducing the real reference reactor. Therefore, simplified 3D models have been adopted, and they will be presented in the following Sections.

2.2 Neutron diffusion equations

The design of a nuclear reactor depends fundamentally on the way in which neutrons interact with matter. It is important to recognise that since neutrons are electrically neutral they pass through the atomic electron cloud and interact directly with the nuclei. Neutrons may interact with nuclei in many ways:[†] the neutron might be absorbed[‡], or it might be scattered via an elastic – or anelastic – collision and consequently looses a fraction of its energy, or the neutron may induce the fission reaction. The probability of such reactions are expressed by the macroscopic cross section Σ for the corresponding reaction, which is a probability of interaction per unit length. Hence, there will be a macroscopic cross section for the absorption, for the fission and scattering reactions. The value of Σ depends on both the nucleus, hit by the neutron, and the energy of the neutron itself. When a fission reaction occurs, some neutrons are immediately emitted – the *prompt* neutrons –

[†]A detailed presentation of the neutron-matter interaction is beyond the aim of the present work. Therefore, other nuclear reactions that might take place such as (n,α), $(n,2n)$ are not mentioned. The interested reader may refer to [18–20].

[‡]Actually, for each nuclear reaction, the neutron is firstly captured by the nucleus and then the nuclear reaction happens. In the present paper, with absorption reaction it is meant that the neutron is absorbed by the nucleus through a radiative capture (n,γ), and an isotope is created.

other are emitted with a delay – the *delayed* neutrons – by the decay of some precursors, which are formed by the splitting of the nucleus via the fission reaction. The neutrons emitted via fission reaction have, on average, a kinetic energy of $\sim$2MeV. However, most of the fission reactions happen when the neutron has been *thermalized*, i.e. its energy is below 0.025 eV. The fission reaction chain, which is fostered by the neutrons, is the engine of the nuclear reactor. Therefore, it is important to model neutrons behaviour within the nuclear reactor core. In nuclear engineering field, the quantity of interest related to the neutrons is the so called *neutron flux* $\Phi(\mathbf{r},t)$ measured in neutrons/cm^{2}s. In fact, when the number of neutrons emitted is equal to the neutrons that are absorbed or that exit the core, the neutron flux is stationary. Conversely, when the neutrons emitted are higher (lower) the neutron flux goes up (down).

As stated in the Introduction, the so called multi-group diffusion theory [5] has been employed. According to this approximation, the spectrum of the neutron energy is split into groups and, for each group, equivalent cross sections are computed that are constant in the energy range of the group. In particular, two energy groups and eight groups of precursors (c_i), where c_i is the concentration of the i-th precursor group, have been employed leading to a set of ten coupled parabolic equations, reported below in their strong formulation.[§]

$$\frac{1}{\mathrm{v}_1}\frac{\partial \Phi_1}{\partial t} = \nabla\cdot(D_1\nabla\Phi_1) + \left[(1-\beta)\nu\Sigma_{f_1} - \Sigma_{a_1} - \Sigma_{s_{1\to 2}}\right]\Phi_1 + \left[(1-\beta)\nu\Sigma_{f_2} + \Sigma_{s_{2\to 1}}\right]\Phi_2 + \sum_{i=1}^{8}\lambda_i c_i, \tag{2.1}$$

$$\frac{1}{\mathrm{v}_2}\frac{\partial \Phi_2}{\partial t} = \nabla\cdot(D_2\nabla\Phi_2) + \Sigma_{s_{1\to 2}}\Phi_1 - \left[\Sigma_{a_2} + \Sigma_{s_{2\to 1}}\right]\Phi_2, \tag{2.2}$$

$$\frac{\partial c_i}{\partial t} = -\lambda_i c_i + \beta_i\left[\nu\Sigma_{f_1}\Phi_1 + \nu\Sigma_{f_2}\Phi_2\right], i=1,\ldots,8, \tag{2.3}$$

with a given initial condition

$$\Phi_1(t=0) = \Phi_1^0, \quad \Phi_2(t=0) = \Phi_2^0, \quad c_i(t=0) = c_i^0, \tag{2.4}$$

where the subscript 1 refers to the fast group (i.e., the most energetic group) and 2 to the thermal one; v is the velocity of the neutrons, Φ is the neutron flux, D is the diffusion coefficient, β is the fraction of delayed neutrons and $\beta = \sum_{i=1}^{8}\beta_i$, $\nu\Sigma_f$ are the number of neutrons emitted per fission reaction, Σ_a is the absorption cross section, $\Sigma_{s_{i\to j}}$ is the scattering cross section from group i to group j, λ_i is the decay constant of the precursor group i. It is worth mentioning that the bilinear form associated to the elliptic part of the equations is non-coercive and non-symmetric. Different spatial domains have been defined for the two approaches developed in the present work, however, both of them are

[§]All the parameters and fluxes are spatially dependent, however this dependency has not been reported in order not to further burden the notation.

Table 1: Neutronic parameters generated by means of the SERPENT code.

Parameter	Fuel	Water	Rod
D_1 [cm]	$8.77 \cdot 10^{-1}$	$8.51 \cdot 10^{-1}$	$7.52 \cdot 10^{-1}$
D_2 [cm]	$1.92 \cdot 10^{-1}$	$1.39 \cdot 10^{-1}$	$1.32 \cdot 10^{-1}$
Σ_{a_1} [cm^{-1}]	$4.85 \cdot 10^{-3}$	$5.04 \cdot 10^{-4}$	$7.07 \cdot 10^{-2}$
Σ_{a_2} [cm^{-1}]	$7.53 \cdot 10^{-2}$	$1.70 \cdot 10^{-2}$	$4.57 \cdot 10^{-1}$
$\nu\Sigma_{f_1}$ [cm^{-1}]	$3.65 \cdot 10^{-3}$	0.0	0.0
$\nu\Sigma_{f_2}$ [cm^{-1}]	$1.25 \cdot 10^{-1}$	0.0	0.0
$\Sigma_{s_{1\to2}}$ [cm^{-1}]	$3.02 \cdot 10^{-2}$	$5.34 \cdot 10^{-2}$	$1.36 \cdot 10^{-2}$
$\Sigma_{s_{2\to1}}$ [cm^{-1}]	$3.27 \cdot 10^{-4}$	$2.49 \cdot 10^{-4}$	$5.83 \cdot 10^{-4}$
$1/\mathrm{v}_1$ [s/cm]	$5.87 \cdot 10^{-8}$	$7.58 \cdot 10^{-8}$	$2.61 \cdot 10^{-8}$
$1/\mathrm{v}_2$ [s/cm]	$3.00 \cdot 10^{-6}$	$3.47 \cdot 10^{-6}$	$3.14 \cdot 10^{-6}$

Precursor group	λ [s^{-1}]	β [-]
1	$1.25 \cdot 10^{-02}$	$3.83 \cdot 10^{-04}$
2	$2.83 \cdot 10^{-02}$	$1.34 \cdot 10^{-03}$
3	$4.25 \cdot 10^{-02}$	$9.63 \cdot 10^{-04}$
4	$1.33 \cdot 10^{-01}$	$1.92 \cdot 10^{-03}$
5	$2.92 \cdot 10^{-01}$	$3.08 \cdot 10^{-03}$
6	$6.66 \cdot 10^{-01}$	$8.61 \cdot 10^{-04}$
7	1.63	$7.88 \cdot 10^{-04}$
8	3.55	$2.31 \cdot 10^{-04}$

derived from the TRIGA core, which will be introduced in the following section. For the sake of simplicity, the homogeneous Dirichlet boundary conditions have been employed. The FE discretization of the Eqs. (2.1)–(2.3), adopting the uniform Backward Euler (BE) in time with twenty time intervals of length 5×10^{-4}s, has been assumed as the "truth" solution. All the simulations needed by the RB method, for both the Offline and Online step, have been performed relying on the C++ library `libMesh` [15] within the `rbOOmit` framework [16].

The neutronic parameters (v, D, Σ_a, Σ_s, $\nu\Sigma_f$) have been generated by means of the continuous energy Monte Carlo neutron transport code SERPENT [35], which features group constant generation capabilities – i.e. it is able to compute the equivalent cross sections – using the nuclear data library JEFF 3.1 [17]. The computed parameters are reported in Tab. 1, and such neutronic quantities have been taken constant for all the simulations.

2.2.1 Neutron transport theory

Neutronics is aimed to determine the neutron distribution within the core and the multi-group neutron diffusion equations are probably the most used approximation of the neutron transport equation, which is an integro-differential equation for the neutron angular

flux. In particular, it describes the number of neutrons within a volume that are characterised by a specific energy and are travelling in a specific direction. Such equation is very difficult to be solved for any but the simplest modelled problems (e.g., infinite slab reactor), and there is no possibility of obtaining exact solutions to the energy-dependent neutron transport equation for general reactor problems [2]. Therefore, different suitable approximations (i.e., computationally feasible and accurate) have been proposed. Such approximations tackle the anisotropy of neutron emission in scattering reactions and the energy dependency of the neutronic cross sections. Typically, the angular distribution of the scattered neutrons is expanded as a series of Legendre polynomials leading to the so-called P_N equations, where N is the maximum order considered (P_1 corresponds to the neutron diffusion equation). Another common alternative is to solve the neutron transport equation in a discrete set of directions only. Such method is known as the discrete ordinates or S_N method, where N is the number of directions considered. As far as the cross section energy dependency is concerned, multi-group methods are usually employed. The discussion about the formulation and range of validity of such approximate theories is beyond the aim of the present work. The interested reader might refer to [2,4], and references therein, for more details.

3 Reduced basis method

In this Section, the strategies upon which the Reduced Basis (RB) method relies are firstly recalled. Subsequently, the essential ingredients of the RB for parabolic partial differential equations (herein PDEs), with reference to the multi-group time-dependent neutron diffusion equations, are presented. For a more general complete presentation of the RB method the reader may refer to [26,29,30], and, for the parabolic case, to [10].

3.1 Reduced basis strategies

The philosophy of reduced order methods, such as RB, even if based on Galerkin projection method, is very different with respect to finite element method. In fact, finite element method approximates the exact solution u, which belongs to an *infinite* dimensional space X, of a partial differential equation with $u_{\mathcal{N}}$, that is a piece-wise polynomial approximation, which belongs to a *finite* dimensional space $X_{\mathcal{N}}$. On the other hand, RB approximates $u_{\mathcal{N}}$ with u_N, using a *low* dimensional space X_N. The basis functions (also called shape functions) employed for constructing the space $X_{\mathcal{N}}$ feature "small" support (i.e. the support is given by a few elements of the mesh on which a finite element approximation has been built for this work), and they are *independent* of the problem considered. Conversely, RB employs *ad hoc* built basis functions, whose support is the entire spatial domain, and strictly related to the considered case.

Before going more deeply inside the methodology, the essential ingredients of RB methodology [27], employed in this work, can be summarized as follows: a Galerkin projection onto a low-dimensional space of basis functions properly selected, an affine

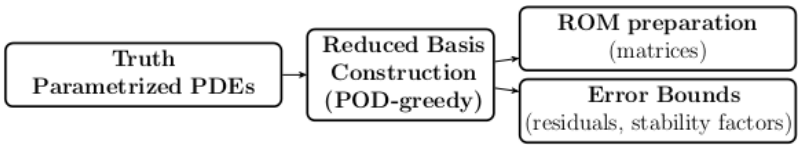

Figure 2: Conceptual flow chart for the Offline step.

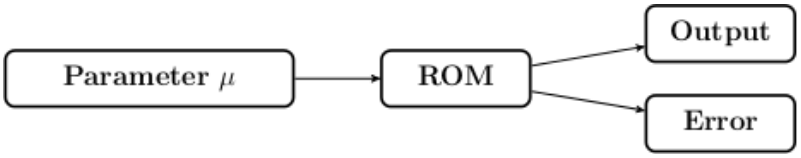

Figure 3: Conceptual flow chart for the Online step.

parametric dependency enabling to perform a competitive Offline-Online splitting in the computational procedure, and a rigorous *a posteriori* error estimation used for both the basis selection and the certification of the solution. The combination of these three factors yields substantial computational savings which are at the basis of an efficient model order reduction, ideally suited for real-time simulation and many-query contexts (for example, optimization, control or parameter identification). It is worth recalling that the rational of this approach stands in the fact that the set of all solutions, as function of the parameters, behaves well [26], or, more precisely, that the Kolmogorov n-width is small [22].

The Offline step can be depicted as in the flow chart reported in Fig. 2. The starting point is the "truth" model, which is a high fidelity finite element approximation of a set of parametrized partial differential equations (PDEs). Relying on a POD-greedy algorithm, which is recalled in Section 3.2.6, the "truth" model is solved for a suitable number of parameter instances, and matrices for the Reduced Order Model (ROM) as well as for error bounds estimation are computed and stored (more details are given in Sections 3.2.3 and 3.2.4, respectively). At the end of this step, the RB method leads to a ROM of the "truth" one, along with an *a posteriori* error estimation for the greedy parameter space exploration and basis functions selection. The Offline step is performed only once and it may be very expensive in terms of computational burden. Most of the physical information (or energy) of the system is stored in the RB space.

When the ROM is obtained, the Online step consists of the input/output evaluation for a given parameter μ, as shown in Fig. 3. The computational time required to solve the ROM, is usually very short. The gain of the so obtained reduced model can be expressed as the ratio between the time required to solve the "truth" model with respect to the Online step duration. Such gain is referred to as computational speed-up. Finally, the number of basis functions employed can be set Online, so the ROM matrices can have (in the scalar case) dimension $N \times N$, for $N = 1,\dots,N_{\max}$, and $N \leq N_{\max} \ll \mathcal{N}$, where $\mathcal{N}$ is the finite element space dimension of the "truth" model.

3.2 Application to neutron diffusion equations

As shown in Section 2, the neutron kinetics has been described according to the so-called multi-group time-dependent neutron diffusion equation [5], which is a set of coupled parabolic PDEs. Moreover the bilinear form, associated to the elliptical part of the equations, is not symmetric neither coercive. In this work, the movement of the control rod has been parametrized. In the following, the parameter μ refers to the height of the control rods (i.e., how much the rod is inserted within the core), and more details about the models are given in Sections 4 and 5 and in Figs. 5, 6 and 7.

3.2.1 Abstract formulation

A parabolic model problem, parametrized with respect to the input parameter p-vector μ, can be defined as follows [27]: given $\mu \in \mathcal{D} \subset \mathbb{R}^p$, $\forall t \in I = \left[0, t_f\right]$, find $u(t;\mu) \in L^2(I; X(\Omega_o))$ – the subscript o will be clarified in the following – is such that

$$m\left(\frac{\partial u(t;\mu)}{\partial t}, v; \mu\right) + a(u(t;\mu), v; \mu) = f(v), \forall v \in X(\Omega_o), \forall t \in I, \tag{3.1}$$

subject to initial condition $u(0;\mu) = u_0$. Ω_o is a spatial domain in $\mathbb{R}^d$ (for $d = 2$ or 3), $X = X(\Omega_o)$ is a suitable Hilbert space, with a given inner product $(\cdot,\cdot)_X$ and an induced norm $\|\cdot\|_X = \sqrt{(\cdot,\cdot)_X}$. In the considered case $u(t;\mu)$ can be defined as follows:

$$u(t;\mu) = \begin{bmatrix} \Phi_1(t;\mu) \\ \Phi_2(t;\mu) \\ c_1(t;\mu) \\ \vdots \\ c_8(t;\mu) \end{bmatrix}, \tag{3.2}$$

and the test function v as

$$v = \begin{bmatrix} \psi_{\Phi_1} \\ \psi_{\Phi_2} \\ \psi_{c_1} \\ \vdots \\ \psi_{c_8} \end{bmatrix}. \tag{3.3}$$

In the following, the dependency of the neutron flux and precursors on time and parameter μ has to be understood, and it is not reported in order not to overburden the notation. The operators m and a can be formulated as follows:

$$m(u(t;\mu),v) = \int_{\Omega_o(\mu)} \left[\frac{1}{v_1} \frac{\partial \Phi_1}{\partial t} \psi_{\Phi_1} + \frac{1}{v_2} \frac{\partial \Phi_2}{\partial t} \psi_{\Phi_2} + \sum_{i=1}^{8} c_i \psi_{c_i} \right], \tag{3.4}$$

$$\begin{aligned} a(u(t),v) = & \underbrace{\int_{\Omega_o(\mu)} D_1 \nabla \Phi_1 \cdot \nabla \psi_{\Phi_1}}_{a^1} + \underbrace{\int_{\Omega_o(\mu)} D_2 \nabla \Phi_2 \cdot \nabla \psi_{\Phi_2}}_{a^2} + \underbrace{\int_{\Omega_o(\mu)} \Sigma_{a_1} \Phi_1 \psi_{\Phi_1}}_{a^3} \\ & + \underbrace{\int_{\Omega_o(\mu)} \Sigma_{s_{1\to 2}} \Phi_1 \psi_{\Phi_1}}_{a^4} - \underbrace{\int_{\Omega_o(\mu)} (1-\beta) \nu \Sigma_{f_1} \Phi_1 \psi_{\Phi_1}}_{a^5} \\ & - \underbrace{\int_{\Omega_o(\mu)} \Sigma_{s_{2\to 1}} \Phi_2 \psi_{\Phi_1}}_{a^6} - \underbrace{\int_{\Omega_o(\mu)} (1-\beta) \nu \Sigma_{f_2} \Phi_2 \psi_{\Phi_1}}_{a^7} - \underbrace{\int_{\Omega_o(\mu)} \sum_{i=1}^{8} \lambda_i c_i \psi_{\Phi_1}}_{a^8} \\ & - \underbrace{\int_{\Omega_o(\mu)} \Sigma_{s_{1\to 2}} \Phi_1 \psi_{\Phi_2}}_{a^9} + \underbrace{\int_{\Omega_o(\mu)} \Sigma_{a_2} \Phi_2 \psi_{\Phi_2}}_{a^{10}} + \underbrace{\int_{\Omega_o(\mu)} \Sigma_{s_{2\to 1}} \Phi_2 \psi_{\Phi_2}}_{a^{11}} \\ & - \underbrace{\int_{\Omega_o(\mu)} \sum_{i=1}^{8} \beta_i \nu \Sigma_{f_1} \Phi_1 \psi_{c_i}}_{a^{12}} - \underbrace{\int_{\Omega_o(\mu)} \sum_{i=1}^{8} \beta_i \nu \Sigma_{f_2} \Phi_2 \psi_{c_i}}_{a^{13}} \\ & + \underbrace{\int_{\Omega_o(\mu)} \sum_{i=1}^{8} \lambda_i c_i \psi_{c_i}}_{a^{14}}, \end{aligned} \tag{3.5}$$

(3.6)

where ψ is the test function for the corresponding variable. For the neutron fluxes and corresponding test functions $H^1(\Omega_0(\mu))$ Hilbert space has been chosen, whereas the $L^2(\Omega_0(\mu))$ space has been used for the precursors. It is worth pointing out that the bilinear form a is non-symmetric. Moreover, it has been verified that the production terms a^7 and a^8 make the bilinear form non-coercive, for the values of the neutronic quantities reported in Tab 1. In order to have a stationary neutron flux distribution when the reactor is subcritical (i.e., when the number of neutrons produced is lower than the number of neutrons absorbed), a uniform source, equal to 1 neutron/cm^{2}s, within the fuel has been considered. In weak formulation, it reads

$$f(v) = \int_{\Omega_o^{\text{fuel}}} 1 \times \psi_{\Phi_1}. \tag{3.7}$$

It is assumed that the bilinear forms $a(u(t;\mu),v;\mu)$ and $m(u(t;\mu),v;\mu)$ are continuous

with continuity constants γ and ρ,

$$a(u,v;\mu) \leq \gamma(\mu)\|u\|_X\|v\|_X \leq \gamma_0\|u\|_X\|v\|_X, \forall u,v \in X, \forall \mu \in \mathcal{D}, \tag{3.8}$$

$$m(u,v;\mu) \leq \rho(\mu)\|u\|_X\|v\|_X \leq \rho_0\|u\|_X\|v\|_X, \forall u,v \in X, \forall \mu \in \mathcal{D}. \tag{3.9}$$

Finally, it is assumed that a and m depend *affinely* on the parameter μ, hence they can be expressed as

$$a(u,v;\mu) = \sum_{q=1}^{Q_a} \Theta_a^q(\mu) a^q(u,v), \quad \forall u,v \in X, \forall \mu \in \mathcal{D}, \tag{3.10}$$

$$m(u,v;\mu) = \sum_{q=1}^{Q_m} \Theta_m^q(\mu) m^q(u,v), \quad \forall u,v \in X, \forall \mu \in \mathcal{D}, \tag{3.11}$$

for some integers Q_a and Q_m. The coefficients of the affine expansions (3.10) and (3.11) can be easily derived when they are related to physical properties (e.g., diffusion coefficients, thermal conductivity). Whether the μ-vector includes geometric properties, the derivation of the $\Theta(\mu)$ coefficients may require a dedicated treatment. When affine parameter dependency is not holding, as well as in case of non-linearities, an equivalent recovered affine formulation (to allow offline-online computational decomposition) can rely on a well established Empirical Interpolation Method [1].

3.2.2 Geometric parametrization

Let $\Omega_o(\mu)$ be a parametrized spatial domain, which is called *original* domain. The RB framework requires also a *reference* (μ-independent) domain $\Omega = \Omega_o(\mu_{\text{ref}})$ in order to compare, and combine, FE solutions that would be otherwise computed on different domains and grids. For this reason, $\Omega_o(\mu)$ has to be mapped to Ω in order to get the *transformed* problem, which is the point of departure of the RB approach[¶]. In order to build a parametric mapping related to geometrical properties, a conforming domain decomposition of $\Omega_o(\mu)$ has to be introduced

$$\Omega_o(\mu) = \bigcup_{l=1}^{L_{\text{dom}}} \Omega_o^l(\mu), \tag{3.12}$$

consisting of mutually non-overlapping open subdomains $\Omega_o^l(\mu)$, such that $\Omega_o^l(\mu) \cap \Omega_o^{l'}(\mu) = \emptyset$, $1 \leq l < l' \leq L_{\text{dom}}$. Original and reference subdomains must be linked *via* a mapping $\mathcal{T}(\cdot;\mu) : \Omega^l \to \Omega_o^l(\mu)$, $1 \leq l \leq L_{\text{dom}}$ such that

$$\Omega_o^l(\mu) = \mathcal{T}^l(\Omega^l;\mu), 1 \leq l \leq L_{\text{dom}}. \tag{3.13}$$

These maps must be individually bijective, collectively continuous, and such that

$$\mathcal{T}^l(\mathbf{x};\mu) = \mathcal{T}^{l'}(\mathbf{x};\mu), \forall \mathbf{x} \in \Omega^l \cap \Omega^{l'}, 1 \leq l < l' \leq L_{\text{dom}}. \tag{3.14}$$

[¶]From finite element consolidated fashion, such mapping may be seen as the isoparametric transformation from the original mesh element to the reference element to perform the Gaussian integration.

In this work, the following affine transformation, for $\mu \in \mathcal{D}$ and $\mathbf{x} \in \Omega^l$, has been employed

$$\mathcal{T}_i^l(\mathbf{x};\mu) = C_i^l(\mu) + \sum_{j=1}^{d} G_{ij}^l(\mu) x_j, \qquad 1 \le i \le d, \tag{3.15}$$

for given translation vector $C^l : \mathcal{D} \to \mathbb{R}^d$ and linear transformation matrices $G^l : \mathcal{D} \to \mathbb{R}^{d \times d}$. The following terms, which will be useful later on, can be defined

$$J^l(\mu) = |\det(G^l(\mu))|, \qquad 1 \le l \le L_{\text{dom}}, \tag{3.16}$$

$$D^l(\mu) = (G^l(\mu))^{-1}, \qquad 1 \le l \le L_{\text{dom}}. \tag{3.17}$$

The class of admissible operators, which allow an affine expansion for a geometric parametrization, can be expressed by the following associated bilinear forms [30]

$$a_o(w,\psi;\mu) = \sum_{l=1}^{L_{\text{dom}}} \int_{\Omega_o^l(\mu)} \left[\frac{\partial w}{\partial x} \frac{\partial w}{\partial y} \frac{\partial w}{\partial z} w \right] \mathcal{K}_o^l(\mu) \begin{bmatrix} \dfrac{\partial \psi}{\partial x} \\ \dfrac{\partial \psi}{\partial y} \\ \dfrac{\partial \psi}{\partial z} \\ \psi \end{bmatrix}, \tag{3.18}$$

where, w is a generic variable (e.g., Φ_1, c_1, etc.), ψ the corresponding test function, $\mathcal{K}_o^l : \mathcal{D} \to \mathbb{R}^{(d+1)\times(d+1)}, 1 \le l \le L_{\text{dom}}$, are prescribed coefficients. In particular, the upper $d \times d$ principal submatrix of $\mathcal{K}_o^l$ is the matrix of diffusivity; the $(d+1,d+1)$ element of $\mathcal{K}_o^l$ represents the reaction terms; the other terms are set to zero. For example, substituting w and ψ with Φ_1 and ψ_{Φ_1}, respectively, the $\mathcal{K}_o^l$ can be expressed as follows:

$$\mathcal{K}_o^l = \begin{bmatrix} D_1 & 0 & 0 & 0 \\ 0 & D_1 & 0 & 0 \\ 0 & 0 & D_1 & 0 \\ 0 & 0 & 0 & \Sigma_{a_1} + \Sigma_{s_{1\to 2}} - (1-\beta)\nu\Sigma_{f_1} \end{bmatrix}. \tag{3.19}$$

In addition, the following relation has to be considered as well

$$m_o(w,\psi;\mu) = \sum_{l=1}^{L_{\text{dom}}} \int_{\Omega_o^l(\mu)} w \mathcal{M}_o^l(\mu) \psi, \tag{3.20}$$

where $\mathcal{M}_o^l : \mathcal{D} \to \mathbb{R}$ represents the identity operator. By identifying $u(t;\mu) = u_o(t;\mu) \circ \mathcal{T}(\cdot;\mu) \forall t > 0$, and tracing (3.18) back to the reference domain Ω by the mapping $\mathcal{T}(\cdot;\mu)$,

it follows that the bilinear form $a(w,\psi;\mu)$ can be expressed as

$$a(w,\psi;\mu)=\sum_{l=1}^{L_{\text{dom}}}\int_{\Omega^l}\left[\frac{\partial w}{\partial x}\,\frac{\partial w}{\partial y}\,\frac{\partial w}{\partial z}\,w\right]\mathcal{K}^l(\mu)\begin{bmatrix}\dfrac{\partial\psi}{\partial x}\\ \dfrac{\partial\psi}{\partial y}\\ \dfrac{\partial\psi}{\partial z}\\ \psi\end{bmatrix}, \tag{3.21}$$

where $\mathcal{K}^l:\mathcal{D}\to\mathbb{R}^{4\times4}$ is given by

$$\mathcal{K}^l(\mu)=J^l(\mu)\mathcal{G}^l(\mu)\mathcal{K}^l_o(\mu)\left(\mathcal{G}^l(\mu)\right)^T, \tag{3.22}$$

and

$$\mathcal{G}^l(\mu)=\begin{bmatrix}D^l(\mu) & \mathbf{0}\\ \mathbf{0} & 1\end{bmatrix}. \tag{3.23}$$

Similarly, the transformed bilinear form $m(\cdot,\cdot;\mu)$ can be expressed as

$$m(w,\psi;\mu)=\sum_{l=1}^{L_{\text{dom}}}\int_{\Omega_l} w\mathcal{M}^l\psi, \tag{3.24}$$

where $\mathcal{M}^l:\mathcal{D}\to\mathbb{R}$ is given by

$$\mathcal{M}^l(\mu)=J^l(\mu)\mathcal{M}^l_o(\mu). \tag{3.25}$$

At this point, the original problem has been reformulated on the reference domain, resulting in a parametrized problem where the effect of geometry variations is traced back onto its parametrized transformation tensors. For example, the affine formulation (3.10) can be derived by expanding the expression (3.21) in terms of the subdomains Ω_l and the different entries of $\mathcal{K}^l_{ij}$ leading to

$$a(w,\psi;\mu)=\mathcal{K}^1_{11}(\mu)\int_{\Omega_1}\frac{\partial w}{\partial x}\,\frac{\partial\psi}{\partial x}+\mathcal{K}^1_{22}(\mu)\int_{\Omega_1}\frac{\partial w}{\partial y}\,\frac{\partial\psi}{\partial y}+\dots \tag{3.26}$$

It is worth pointing out that $\mathcal{K}^l$ can be non-diagonal even if $\mathcal{K}^l_o$ is diagonal.

3.2.3 Construction of the reduced basis approximation

The RB method is built upon a fine approximation (i.e., finite element or finite volume), assumed as "truth" solution. This implies that the error of the RB solution is estimated with respect to the fine approximation. The error of the "truth" solution, with respect to the "exact" solution, is inherited by the ROM. Let the following expression be the

discretization of the parabolic problem (3.1) adopting the finite difference in time, using the Backward Euler (BE) method, and Finite Element (FE) [28] in space

$$\begin{aligned}&\frac{1}{\Delta t}m(u^k(\mu)-u^{k-1}(\mu),v;\mu)+a(u^k(\mu),v;\mu)\\&\quad=f(v),\quad \forall v\in X^{\mathcal{N}},1\le k\le K,\end{aligned}\tag{3.27}$$

subject to initial condition $(u^0,v)=(u_0,v),\forall v\in X^{\mathcal{N}}$, where the time interval I has been divided into K subintervals of equal length $\Delta t=t_f/K$, $t^k=k\Delta t$, and $X^{\mathcal{N}}$ is the FE approximation space of dimension $\mathcal{N}$ (usually very large).

Then, given a positive integer $N_{\max}$, let X_N, for $N=1,\dots,N_{\max}$, be an associated sequence of approximation spaces (RB spaces), where X_N is a N-dimensional subspace of $X^{\mathcal{N}}$. The RB spaces are such that they are *hierarchical*

$$X_1\subset X_2\subset\cdots\subset X_{N_{\max}}\subset X^{\mathcal{N}}.\tag{3.28}$$

The RB approximation of the discretized parabolic problem (3.27) can be stated as follows

$$\begin{aligned}&\frac{1}{\Delta t}m(u_N^k(\mu)-u_N^{k-1}(\mu),v;\mu)+a(u_N^k(\mu),v;\mu)\\&\quad=f(v),\quad \forall v\in X_N,1\le k\le K,\end{aligned}\tag{3.29}$$

subject to initial condition $(u_N^0,v)=(u_0,v),\forall v\in X_N$. Let $\xi_n^{\mathcal{N}}\in X^{\mathcal{N}},1\le n\le N_{\max}$ be a set of orthonormal functions and let such functions be the basis of the RB spaces

$$X_N=\operatorname{span}\left\{\xi_n^{\mathcal{N}},1\le n\le N\right\},\quad 1\le N\le N_{\max}.\tag{3.30}$$

The RB approximation $u_N^k(\mu)\in X_N$ can be expressed as

$$u_N^k(\mu)=\sum_{i=1}^{N}u_{N,i}^k(\mu)\xi_i^{\mathcal{N}}.\tag{3.31}$$

Then, by denoting

$$\mathcal{Z}=\left[\xi_1^{\mathcal{N}}|\dots|\xi_N^{\mathcal{N}}\right]\in\mathbb{R}^{\mathcal{N}\times N},\quad 1\le N\le N_{\max},\tag{3.32}$$

the bilinear forms a^q and m^q can be projected onto the RB space X_N as follows

$$\mathbf{A}_N^q=\mathcal{Z}^T A_{\mathcal{N}}^q\mathcal{Z},\tag{3.33}$$

$$\mathbf{M}_N^q=\mathcal{Z}^T M_{\mathcal{N}}^q\mathcal{Z},\tag{3.34}$$

$$\mathbf{f}_N=\mathcal{Z}^T F_{\mathcal{N}},\tag{3.35}$$

where

$$\left(A_{\mathcal{N}}^q\right)_{ij}=a^q(\psi_j,\psi_i),\tag{3.36}$$

$$\left(M_{\mathcal{N}}^q\right)_{ij}=m^q(\psi_j,\psi_i),\tag{3.37}$$

$$\left(F_{\mathcal{N}}\right)_i=f(\psi_i),\tag{3.38}$$

being $\{\psi_i\}_{i=1}^{\mathcal{N}}$ the basis of the FE space $X^{\mathcal{N}}$. Hence, the following algebraic equations associated to the parabolic problem (3.29) are obtained

$$\left[\sum_{q=1}^{Q_a}\Theta_a^q(\mu)\mathbf{A}_n^q+\frac{1}{\Delta t}\sum_{q=1}^{Q_m}\Theta_m^q(\mu)\mathbf{M}_n^q\right]\mathbf{u}_N(t^k;\mu)$$
$$=\mathbf{f}_N+\frac{1}{\Delta t}\sum_{q=1}^{Q_m}\Theta_m^q(\mu)\mathbf{M}_n^q\,\mathbf{u}_N(t^{k-1};\mu), \tag{3.39}$$

where $\left(\mathbf{u}_N(t^k;\mu)\right)_i=u_{N,i}^k(\mu)$. It is worth mentioning that the linear system (3.39), which is $N\times N$, is independent of the FE space dimension $\mathcal{N}$, and $N\ll\mathcal{N}$. This means that the size of the reduced model does not depend on the mesh of the "truth" problem, but on the number of bilinear forms a^q and m^q and the number of basis functions.

3.2.4 A posteriori error estimation

Effective *a posteriori* error bounds for field variables and outputs of interest are crucial for both the efficiency and the reliability of RB approximations [27]. The first ingredient is the dual norm of the residual

$$\varepsilon_N(t^k;\mu)=\sup_{v\in X^{\mathcal{N}}}\frac{r_N(v;t^k;\mu)}{\|v\|_X},\quad 1\le k\le K, \tag{3.40}$$

where $r_N(v;t^k;\mu)$ is the residual associated with the RB approximation (3.29) and it is given by

$$r_N(v;t^k;\mu)=f(v)-\frac{1}{\Delta t}m\left(u_N^k(\mu)-u_N^{k-1}(\mu),v;\mu\right)$$
$$-a(u_N^k(\mu),v;\mu),\quad \forall v\in X^{\mathcal{N}},1\le k\le K. \tag{3.41}$$

The second ingredient is a lower bound for the inf-sup constant $\beta_{\text{inf}-\text{sup}}^{\mathcal{N}}(\mu)$ (see Section 3.2.5), associated to the non-coercive operator, such that

$$0<\beta_{\text{LB}}^{\mathcal{N}}(\mu)\le\beta_{\text{inf}-\text{sup}}^{\mathcal{N}}(\mu),\quad \forall\mu\in\mathcal{D}. \tag{3.42}$$

The error bounds can thus be defined [27] for all $\mu\in\mathcal{D}$ and all N

$$\|u^k(\mu)-u_N^k(\mu)\|_\mu\le\Delta_N^k(\mu)\quad 1\le k\le K, \tag{3.43}$$

where $\Delta_N^k(\mu)\equiv\Delta_N(t^k;\mu)$ is given by

$$\Delta_N^k(\mu)=\left(\frac{\Delta t}{\beta_{\text{LB}}^{\mathcal{N}}(\mu)}\sum_{m=1}^{k}\varepsilon_N^2(t^m;\mu)\right)^{1/2}. \tag{3.44}$$

The above presented error bounds are without any utility if not accompanied by an Offline-Online computational approach, which is an equivalent formulation of (3.39). To begin with [24], the residual equation (3.41) can be rewritten according to the affine expansion, Eqs. (3.10) and (3.11), and the reduced basis representation (3.31)

$$r_N(v,t^k;\mu) = f(v) - \frac{1}{\Delta t}\sum_{q=1}^{Q_m}\sum_{i=1}^{N}\Theta_m^q(\mu)\left[u_{N,i}^k(\mu) - u_{N,i}^{k-1}(\mu)\right] m^q(\xi_i^{\mathcal{N}},v) - \sum_{q=1}^{Q_a}\sum_{i=1}^{N}\Theta_a^q(\mu)\left[u_{N,i}^k(\mu) - u_{N,i}^{k-1}(\mu)\right] a^q(\xi_i^{\mathcal{N}},v), \tag{3.45}$$

for $1 \le k \le K$. It shall prove convenient to introduce the Riesz representation of $r_N(v,t^k;\mu)$: $\hat{e}_N(t^k;\mu) \in X^{\mathcal{N}}$ satisfies

$$\left(\hat{e}_N(t^k;\mu),v\right)_X = r_N(v;t^k;\mu), \quad \forall v \in X^{\mathcal{N}}. \tag{3.46}$$

It now follows directly from (3.46) and (3.45) that

$$\hat{e}_N(t^k;\mu) = \Gamma + \frac{1}{\Delta t}\sum_{q=1}^{Q_m}\sum_{i=1}^{N}\Theta_m^q(\mu)\left[u_{N,i}^k(\mu) - u_{N,i}^{k-1}(\mu)\right]\Lambda_N^{q,i} + \sum_{q=1}^{Q_a}\sum_{i=1}^{N}\Theta_a^q(\mu)\left[u_{N,i}^k(\mu) - u_{N,i}^{k-1}(\mu)\right]\Upsilon_N^{q,i}, \tag{3.47}$$

where

$$(\Gamma,v)_X = f(v), \quad \forall v \in X^{\mathcal{N}}, \tag{3.48}$$

$$(\Lambda_N^{q,i},v)_X = -m^q(\xi_i^{\mathcal{N}},v), \quad \forall v \in X^{\mathcal{N}}, \quad 1 \le q \le Q_m, \quad 1 \le i \le N, \tag{3.49}$$

$$(\Upsilon_N^{q,i},v)_X = -a^q(\xi_i^{\mathcal{N}},v), \quad \forall v \in X^{\mathcal{N}}, \quad 1 \le q \le Q_a, \quad 1 \le i \le N. \tag{3.50}$$

For duality arguments, the $\varepsilon_N(t^k;\mu)$ can be expressed as

$$\varepsilon_N^2(t^k;\mu) = \|\hat{e}_N(t^k;\mu)\|_X^2, \quad 1 \le k \le K. \tag{3.51}$$

Substituting Eq. (3.47) into the above expression follows that

$$\begin{aligned}\varepsilon_N^2(t^k;\mu) = {} & C^{ff} + \sum_{i=1}^{N}\sum_{j=1}^{N}u_{N,i}^k(\mu)u_{N,j}^k(\mu)C_{Ni,j}^{aa}(\mu) \\ & + \frac{1}{\Delta t^2}\sum_{i=1}^{N}\sum_{j=1}^{N}\left[u_{N,i}^k(\mu) - u_{N,i}^{k-1}(\mu)\right]\left[u_{N,j}^k(\mu) - u_{N,j}^{k-1}(\mu)\right]C_{Ni,j}^{mm}(\mu) \\ & + 2\sum_{i=1}^{N}u_{N,i}^k(\mu)C_{Ni}^{fa}(\mu) + \frac{2}{\Delta t}\sum_{i=1}^{N}\left[u_{N,i}^k(\mu) - u_{N,i}^{k-1}(\mu)\right]C_{Ni}^{fm}(\mu) \\ & + \frac{2}{\Delta t}\sum_{i=1}^{N}\sum_{j=1}^{N}\left[u_{N,i}^k(\mu) - u_{N,i}^{k-1}(\mu)\right]u_{N,j}^k(\mu)C_{Ni,j}^{am}(\mu), \quad 1 \le k \le K,\end{aligned} \tag{3.52}$$

where

$$C^{ff} = (\Gamma,\Gamma)_X, \tag{3.53}$$

$$C^{aa}_{Ni,j}(\mu) = \sum_{q=1}^{Q_a}\sum_{q'=1}^{Q_a} \Theta_a^q(\mu)\Theta_a^{q'}(\mu)\left(\Upsilon_N^{q,i},\Upsilon_N^{q',j}\right)_X, \quad 1\le i,j\le N, \tag{3.54}$$

$$C^{mm}_{Ni,j}(\mu) = \sum_{q=1}^{Q_m}\sum_{q'=1}^{Q_m} \Theta_m^q(\mu)\Theta_m^{q'}(\mu)\left(\Lambda_N^{q,i},\Lambda_N^{q',j}\right)_X, \quad 1\le i,j\le N, \tag{3.55}$$

$$C^{fa}_{Ni}(\mu) = \sum_{q=1}^{Q_a} \Theta_a^q(\mu)\left(\Upsilon_N^{q,i},\Gamma\right)_X, \quad 1\le i\le N, \tag{3.56}$$

$$C^{fm}_{Ni}(\mu) = \sum_{q=1}^{Q_m} \Theta_m^q(\mu)\left(\Lambda_N^{q,i},\Gamma\right)_X, \quad 1\le i\le N, \tag{3.57}$$

$$C^{am}_{Ni,j}(\mu) = \sum_{q=1}^{Q_m}\sum_{q'=1}^{Q_a} \Theta_m^q(\mu)\Theta_a^{q'}(\mu)\left(\Lambda_N^{q,i},\Upsilon_N^{q',j}\right)_X, \quad 1\le i,j\le N. \tag{3.58}$$

Therefore, in the Offline phase, $\Gamma,\Lambda_N^{q,i}$ and $\Upsilon_N^{q,i}$ are found and the inner products $(\Gamma,\Gamma)_X$, $\left(\Upsilon_{N_{\max}}^{q,i},\Upsilon_{N_{\max}}^{q',j}\right)_X$, $\left(\Lambda_{N_{\max}}^{q,i},\Lambda_{N_{\max}}^{q',j}\right)_X$, $\left(\Upsilon_{N_{\max}}^{q,i},\Gamma\right)_X$, $\left(\Lambda_{N_{\max}}^{q,i},\Gamma\right)_X$, $\left(\Lambda_{N_{\max}}^{q,i},\Upsilon_{N_{\max}}^{q',j}\right)_X$ are computed.

3.2.5 $\beta_{\text{inf}-\text{sup}}$ stability constant computation

The *inf-sup* condition [27], for a parametrized non-coercive bilinear form $a(\cdot,\cdot;\mu): X^1\times X^2\to\mathbb{R}$, can be formulated as follows:

$$\exists\beta_0>0 : \beta_{\text{inf}-\text{sup}}(\mu) := \inf_{w\in X^1}\sup_{v\in X^2}\frac{a(w,v;\mu)}{\|w\|_{X^1}\|v\|_{X^2}} \ge \beta_0, \quad \forall\mu\in\mathcal{D}. \tag{3.59}$$

This condition can be reformulated [27] in terms of the so-called *inner supremizer* operator $T^\mu: X^1\to X^2$,

$$(T^\mu w,v)_{X^2} = a(w,v;\mu), \quad \forall w\in X^1,\forall v\in X^2; \tag{3.60}$$

by Cauchy-Schwarz inequality and taking $v = T^\mu w$, it follows that for any $w\in X^1$,

$$a(w,T^\mu w;\mu) \ge \beta_{\text{inf}-\text{sup}}(\mu)\|w\|_{X^1}\|T^\mu w\|_{X^2}. \tag{3.61}$$

Equivalently, the $\beta_{\text{inf}-\text{sup}}$ constant can be computed as follows:

$$\beta^2_{\text{inf}-\text{sup}} = \inf_{w\in X^1}\frac{(T^\mu w,T^\mu w)_{X^2}}{\|w\|^2_{X^1}}, \tag{3.62}$$

which is a Rayleigh quotient.

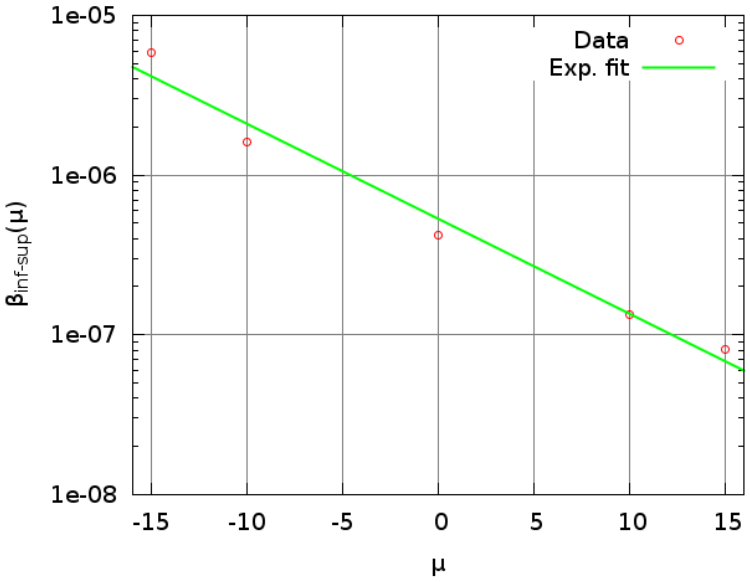

Figure 4: Exponential fit of the $\beta_{\text{inf}-\text{sup}}$ stability constant.

It must pointed out that the computation of the $\beta_{\text{inf}-\text{sup}}(\mu)$ has to be performed only over the symmetric part of the bilinear form $a(\cdot,\cdot)$ and it is very expensive and not suited for Online computing. The reader may refer to [14, 27] for some examples.

Usually, the Successive Constraint Method (SCM) [13, 14] is used in order to provide accurate and inexpensive approximations of a lower bound for the $\beta_{\text{inf}-\text{sup}}(\mu)$ ($\beta_{\text{LB}}(\mu)$). However, different approaches may be considered as well (e.g., [21]). Indeed, in the present work, surrogate models for the $\beta_{\text{inf}-\text{sup}}(\mu)$ have been developed by interpolating over a suitable set of values of $\beta_{\text{inf}-\text{sup}}(\mu)$ obtained solving the generalized eigenvalue problem (3.62). In Fig. 4, the exponential fit of the computed $\beta_{\text{inf}-\text{sup}}(\mu)$ is reported as function of the parameter μ, which is the height of the control rod*.

3.2.6 Sampling strategy: POD-greedy approach

During the Offline phase the RB approximation space X_N is built using a POD-greedy procedure [11, 25, 27]: the greedy algorithm selects for whom μ_i^* the FE system (3.1) is solved, while the POD (Proper Orthogonal Decomposition [3, 12]) is used to capture the causality associated with the evolution in time of the system. As a result, one or more basis functions $\zeta_i^{\mathcal{N}}(\mu_i^*) \in X^{\mathcal{N}}$ are retained for each μ_i^*. Then, the RB space can be generated

*For the three-rods model, the superposition of the effects has been hypothesized to hold, i.e. the three rods have been assumed as independent. Actually, there is a sort of "control rod shadowing" [19], meaning that the effect induced by one rod may rely on the positions of the other rods. However, the hypotheses entered in the derivation of the model itself introduce errors, with respect to the real phenomena, that are more important than this one. Therefore, the "control rod shadowing" has been considered negligible for the purposes of the present work.

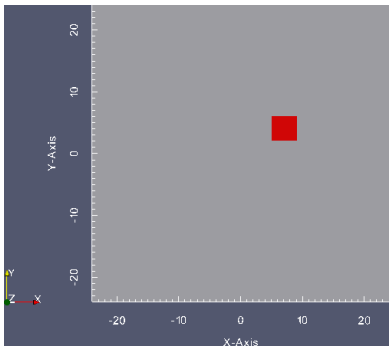

(a) $x-y$ cross section view.

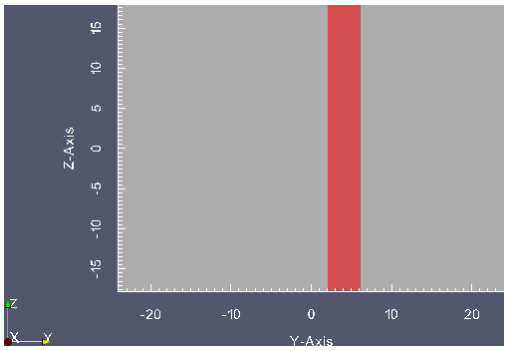

(b) $y-z$ cross section view.

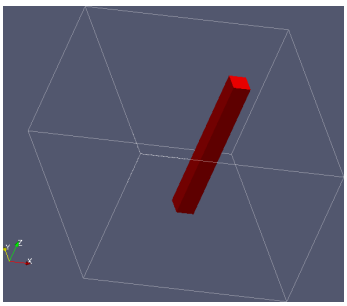

(c) 3D view of the control rod volume.

Figure 5: Simplified 3D model employed.

as

$$X_N = \text{span}\left\{\zeta_i^{\mathcal{N}}, 1 \leq i \leq N\right\}. \tag{3.63}$$

Such procedure is performed iteratively until either $N = N_{\max}$ or when the error bound $\Delta_N^K(\mu)$ is beyond a threshold ε^*, where both $N_{\max}$ and ε^* are given by the user (see, for example, [25]). In this way, a uniform rapid convergence over the parameter domain is provided [27].

4 One rod 3D modelling: piece-wise affine transformation

The RB method has been applied to model the parametrized movement of a control rod (the SHIM rod, see Fig. 1) in a 3D simplified domain of the TRIGA Mark II reactor.[†] The considered model is reported in Figs. 5a and 5b, where the position of the control rod is

[†]This work can be considered also an improvement and extension of the previous work [32]. Indeed, a 3D framework and a different technique for the estimation of the stability constant $\beta_{\text{inf}-\text{sup}}$ have been employed (see Section 3.2.5).

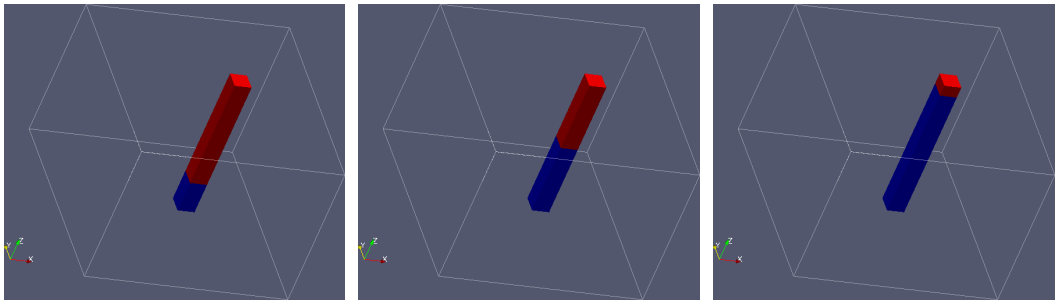

(a) (b) (c)

Figure 6: Three different positions of the control rod, in red, followed by water, in blue.

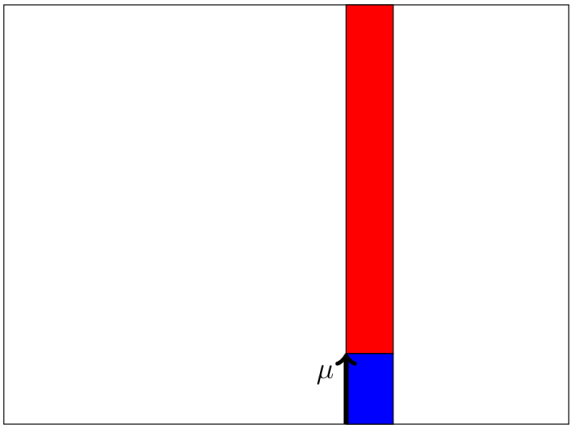

Figure 7: $y-z$ view of the parametrized domain.

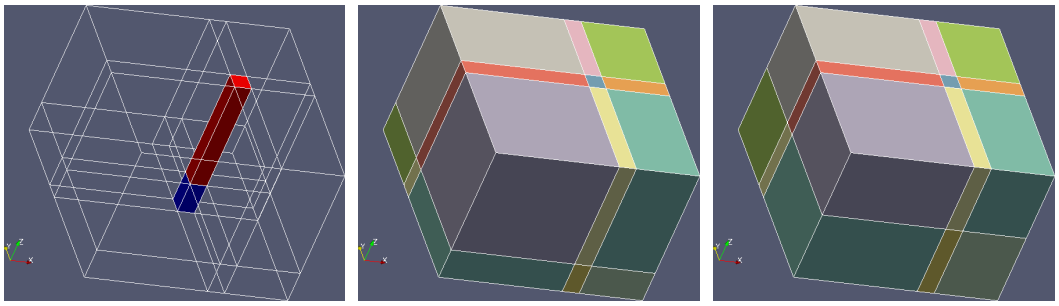

(a) (b) (c)

Figure 8: Domain decomposition of: the original domain with $\mu = -10$cm (a) and (b); reference domain (c).

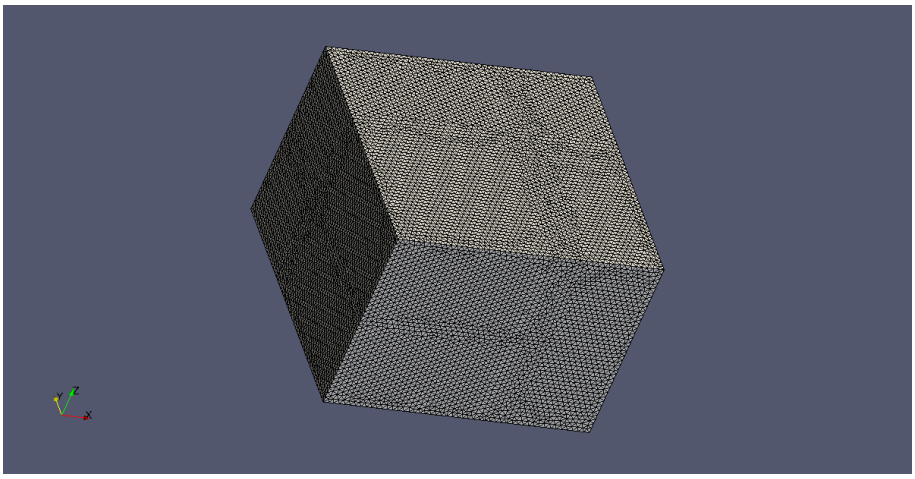

Figure 9: Spatial mesh adopted for the one rod model.

highlighted in red. The rod is surrounded by a fissile material. In particular, a rectangular parallelepiped of dimension $48\,\text{cm} \times 48\,\text{cm} \times 35.6\,\text{cm}$ has been considered, where a control rod, having square basis of side equal to 2 cm, is placed in a non-symmetric position. Figure 5c highlights the portion of the domain where the control rod can move. When the rod is withdrawn, its volume is filled by water. Figure 6 shows an example of three different configurations that the developed model has to handle in a rapid and reliable way, when the height of the rod (i.e., the parameter $\mu \in [-16,16]$ cm) is set in the Online phase. To this aim, the $y-z$ view of the parametrized geometry is reported in Fig. 7. The movement of the rod has been modelled according to a piecewise affine transformation based on subdomain division [30]. In order to guarantee the continuity between elements of the mesh, the original domain has to be divided in suitable subdomains. In Fig. 8, the original domain, when $\mu = 10$cm, is reported with the corresponding subdomain decomposition. As stated in the Section 3.2.2, the RB framework requires also a reference (μ-independent) domain in order to compare, and combine, finite element solutions that would be otherwise computed on different domains and grids. The reference domain has been chosen with $\mu = 0$, and it is depicted in Fig. 8c. The reference domain has been discretized using $P1$-elements by means of the Gmsh mesh generator [8]. The mesh, which is shown in Fig. 9, is made up by 365362 elements, with a mesh size of $\sim 6\,\text{mm}$. When the "truth" model has been solved, a tolerance of 1×10^{-9} has been set.

According to the adopted subdomain splitting, the variation of the original subdomains with respect to the reference ones are simply stretching deformations. Therefore, the affine transformation (3.15) can be computed as described in Appendix A, choosing four points that do not belong to the same plane, among the vertices of the subdomain.

4.1 Parametrized formulation

As already pointed out, the varying parameter is the height of the control rod position $\mu \in [-16,16]$ cm. Such parameter, according to the piece-wise affine transformation based on subdomain division, does not explicitly enter in the equations, but in the shape of the subdomains $\Omega_o^l(\mu)$, as reported in Section 3.2.2. For each subdomain $\Omega_o^l(\mu)$, the following bilinear forms have been defined

$$m_l(u,v;\mu) = \int_{\Omega_o^l(\mu)} \left[\frac{1}{\mathrm{v}_1}\Phi_1\psi_{\Phi_1} + \frac{1}{\mathrm{v}_2}\Phi_2\psi_{\Phi_2} + \sum_{i=1}^{8} c_i\psi_{c_i} \right], \tag{4.1}$$

$$\begin{aligned} a_l^1(u,v;\mu) = & \int_{\Omega_o^l(\mu)} \left[D_1 \frac{\partial\Phi_1}{\partial x}\frac{\partial\psi_{\Phi_1}}{\partial x} + D_2 \frac{\partial\Phi_2}{\partial x}\frac{\partial\psi_{\Phi_2}}{\partial x} \right] \\ & + \int_{\Omega_o^l(\mu)} \left[D_1 \frac{\partial\Phi_1}{\partial y}\frac{\partial\psi_{\Phi_1}}{\partial y} + D_2 \frac{\partial\Phi_2}{\partial y}\frac{\partial\psi_{\Phi_2}}{\partial y} \right] \\ & + \int_{\Omega_o^l(\mu)} \left[\Sigma_{a_1} + \Sigma_{s_{1\to 2}} - (1-\beta)\nu\Sigma_{f_1} \right] \Phi_1\psi_{\Phi_1} \\ & - \int_{\Omega_o^l(\mu)} \left[\Sigma_{s_{2\to 1}} + (1-\beta)\nu\Sigma_{f_2} \right] \Phi_2\psi_{\Phi_1} \\ & - \int_{\Omega_o^l(\mu)} \sum_{i=1}^{8} \lambda_i c_i \psi_{\Phi_1} - \int_{\Omega_o^l(\mu)} \Sigma_{s_{1\to 2}} \Phi_1\psi_{\Phi_2} \\ & + \int_{\Omega_o^l(\mu)} \left[\Sigma_{a_2} + \Sigma_{s_{2\to 1}} \right] \Phi_2\psi_{\Phi_2} - \int_{\Omega_o^l(\mu)} \sum_{i=1}^{8} \beta_i \nu\Sigma_{f_1} \Phi_1\psi_{c_i} \\ & - \int_{\Omega_o^l(\mu)} \sum_{i=1}^{8} \beta_i \nu\Sigma_{f_2} \Phi_2\psi_{c_i} + \int_{\Omega_o^l(\mu)} \sum_{i=1}^{8} \lambda_i c_i \psi_{c_i}, \end{aligned} \tag{4.2}$$

$$a_l^2(u,v;\mu) = \int_{\Omega_o^l(\mu)} \left[D_1 \frac{\partial\Phi_1}{\partial z}\frac{\partial\psi_{\Phi_1}}{\partial z} + D_2 \frac{\partial\Phi_2}{\partial z}\frac{\partial\psi_{\Phi_2}}{\partial z} \right], \tag{4.3}$$

where ψ is the test function for the corresponding variable. Due to symmetry, the total number of bilinear forms can be reduced. Indeed, all the subdomains belonging to the upper part of the domain are subjected to the same affine transformation. Similarly, all the subdomains of the lower part of the domain undergo the same transformation. Therefore, according to the affine expansions (3.10) and (3.11), $Q_a = 4$ and $Q_m = 2$.

4.2 Representative results

We now consider the main results obtained both during the Offline and Online phases are presented.

4.2.1 Offline phase

During the Offline phase, the RB space is constructed and the "truth" model is projected on it to obtain the ROM, and a *a posteriori* error estimation is provided as well for the

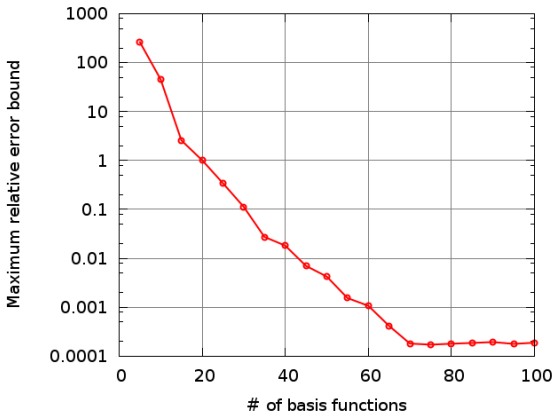

Figure 10: Non-dimensional maximum relative error bound, with respect to the number of basis functions employed.

greedy parameter space exploration and basis functions selection. Figure 10 shows the maximum relative error bound with respect to the number of basis functions employed. After 70 basis functions, the accuracy of the solution provided by the ROM reaches an imposed tolerance.

The value of the parameter for each point in the graph is chosen according to POD-greedy algorithm [11,24,25]. The whole Offline phase lasted almost 20 hours of cpu time on the IBM PLX supercomputer of the Cineca (Italy)[‡].

4.2.2 Online phase

The developed reduced order model has been tested for different values of the parameter μ. In Fig. 11, the flux shape distribution provided by the ROM, employing seventy basis functions, is reported for four different heights of the rod. The corresponding "truth" solutions are depicted in Fig. 12. As it can be seen, the outcomes provided by the ROM are high-fidelity with respect to the "truth" solutions.

As far as the computational time is concerned, in Tab. 2 the times required to solve the "truth" FE problem and the developed ROM for the four values of μ are reported. The proposed reduced model allows an Online computational speed-up of more than 60000 times per single time step per single cpu. Therefore, the Offline step is offset by the achievement of a modelling tool with real-time simulation, which was the goal of the present work. In addition, it must be pointed out that when the reduced model is solved, the *a posteriori* error estimation is performed as well to certify the accuracy of the outcomes. In Tab. 3, the relative error bounds are reported, which have been computed as the ratio between the L^2 norms of the error and the solution (more details about the

[‡]All the calculations have been performed on such supercomputing facility managed by CINECA. Therefore, all the computational times are referred to the above mentioned supercomputer and the reference to it will be omitted in the following.

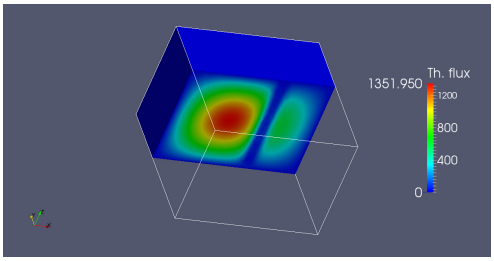

(a) $\mu = -16$cm

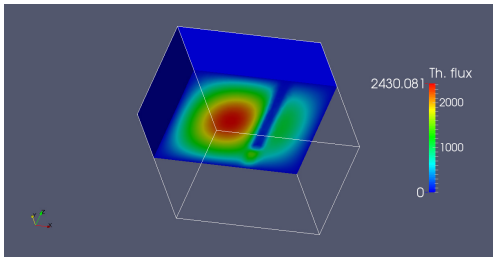

(b) $\mu = -10$cm

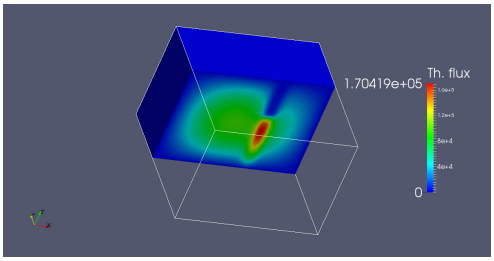

(c) $\mu = 3$cm

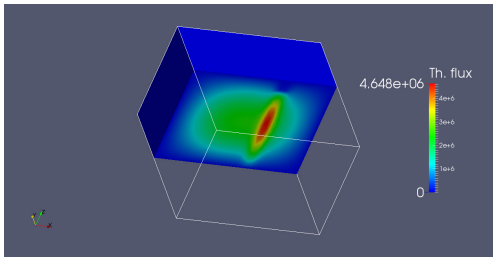

(d) $\mu = 13$cm

Figure 11: Thermal neutron flux shape $[1/\text{cm}^2\text{s}]$ provided by ROM approach, employing $N = 70$ basis functions, at the last time step.

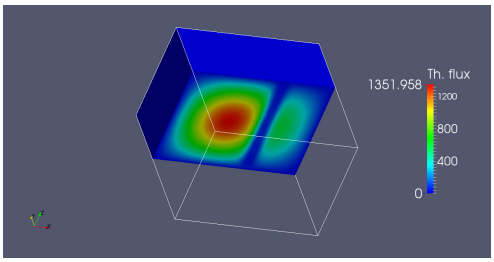

(a) $\mu = -16$cm

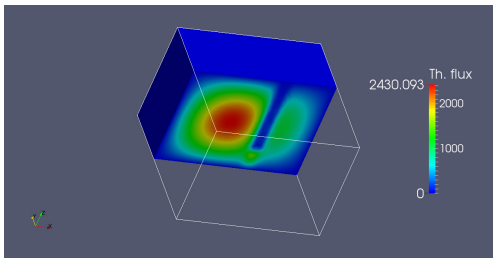

(b) $\mu = -10$cm

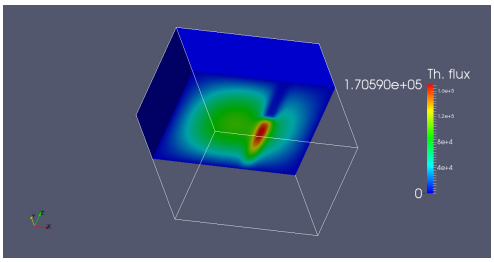

(c) $\mu = 3$cm

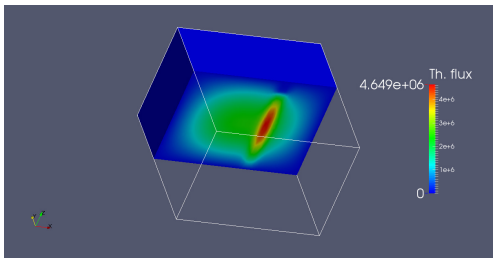

(d) $\mu = 13$cm

Figure 12: Thermal neutron flux shape $[1/\text{cm}^2\text{s}]$ assumed as "truth" solution, at the last time step.

Table 2: Computational time per single cpu per single time step.

	Truth	ROM	Speed-up
$\mu = -16$cm	148.35 s	2.2 ms	67432
$\mu = -10$cm	148.02 s	2.1 ms	70486
$\mu = 3$cm	148.68 s	2.5 ms	59472
$\mu = 13$cm	148.72 s	2.4 ms	61967

Table 3: Relative error bounds in L^2 norm, at the last time step.

	Error bounds
$\mu = -16$cm	9.36×10^{-6}
$\mu = -10$cm	2.48×10^{-4}
$\mu = 3$cm	4.65×10^{-4}
$\mu = 13$cm	1.85×10^{-4}

error bounds can be found in Section 3.2.4). Error bounds are an *estimate* of the error between the RB solution and the high order one. In order to be efficient, the error bounds should overestimate a bit the error and never underestimate it. The ratio between the estimated error with respect to the true error is called *effectivity*. Therefore, the effectivity should be always greater than one but not too big. The average, maximum and minimum effectivity, for 100 instances, randomly sampled, of the parameter, are reported in Tab. 4, where, for the sake of completeness, the influence of the mesh size on the effectivity has been addressed as well. The effectivity parameter increases when the mesh size is increased, on the other hand, when the mesh size is reduced it remains of the same order of magnitude.

For the sake of completeness, it must be introduced the computational break-even, i.e., the number of full order simulations after that the RB method is more efficient and recommended. The break-even can be defined as follows:

$$\text{break-even} = \frac{\text{Whole Offline computational time}}{\text{Time of one FE simulation}} = \frac{\sim 20\,\text{h}}{\sim 8\,\text{min}} = 150. \tag{4.4}$$

Therefore, if more than 150 full-order simulations have to be computed, the reduced order model should be preferred in order to lead to computational savings.

Table 4: Effectivity.

Mesh size	Average	Maximum	Minimum
h=6 mm	17.651	55.036	2.902
h/2	21.806	326.892	2.870
2h	68.493	219.028	14.111
4h	551.009	6941.121	241.542

It is worth recalling that the aim of the present work is to develop a fast-running simulation tool able to accurately reproduce spatial effects induced by the control rods, with respect to the "truth" solutions. To achieve this goal we had to face and incorporate into the computational tool the capability to manage parabolic non-coercive problems, as well as theirs error bounds (and stability factors).

4.3 Additional remarks

The presented methodology, namely the piece-wise affine transformation based on subdomain division, can be used also with multiple rods. In this case, the elementary building block will be tetrahedron and the subdomain shapes will not be simple parallelepipeds as in the presented work and the computation of the affine transformation will be much more involved. Moreover, cylindrical control rods may be employed as well. For example, the cylinder might be inscribed within the parallelepiped, or even curvy-triangles may be considered (see e.g., [30]).

5 Three rods 3D modelling: a "staircase" approach

In this Section, the modelling of three control rod movement is addressed employing a different technique from the previous Section. The geometry of the model considered for this approach is reported in Fig. 13. The TRIGA Mark II reactor is equipped with a pneumatic bar (TRANS), which can be completely inserted or completely withdrawn, without other positions in between. Conversely, the other two rods, REG and SHIM, can assume different positions. The idea behind such approach is to simulate a *discrete* movement (like a staircase). To do so, the portion of the spatial domain (i.e., the three cylinders) occupied by the rods has been divided as shown in Fig. 14. In particular: SHIM and REG, the cylinders have been split into 15 "steps"; TRANS, only 1 big "step". The spatial mesh has been generated by discretizing the domain using the Gmsh software and the $P1$-elements. Such mesh is reported in Fig. 15 and it features 287577 elements, with an average mesh size of $\sim$6 mm. A tolerance of 1×10^{-9} has been chosen for the solution of the "truth" model.

The movement is simulated by "turning on" or "turning off" the water (or the rod) within each "step". According to this kind of approach, the parameters are the height of the control rods (REG and SHIM), which are discrete – from 0, inserted, to 15, withdrawn – and if the TRANS is inserted or withdrawn, namely 0 or 1. Therefore, the following bilinear forms have been defined:[§]

[§]Since the domain does not change, like in the previous Section, the subscript o will be omitted.

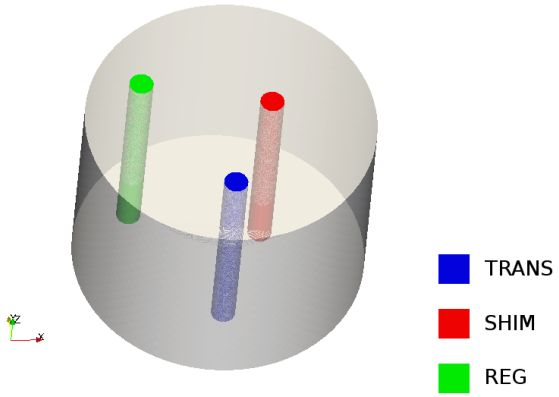

Figure 13: 3D model of the TRIGA reactor with three control rods.

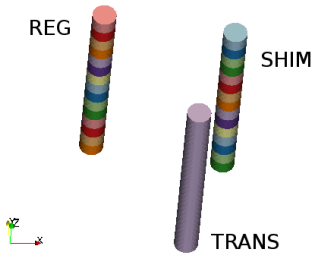

Figure 14: Control rods spatial domain subdivision.

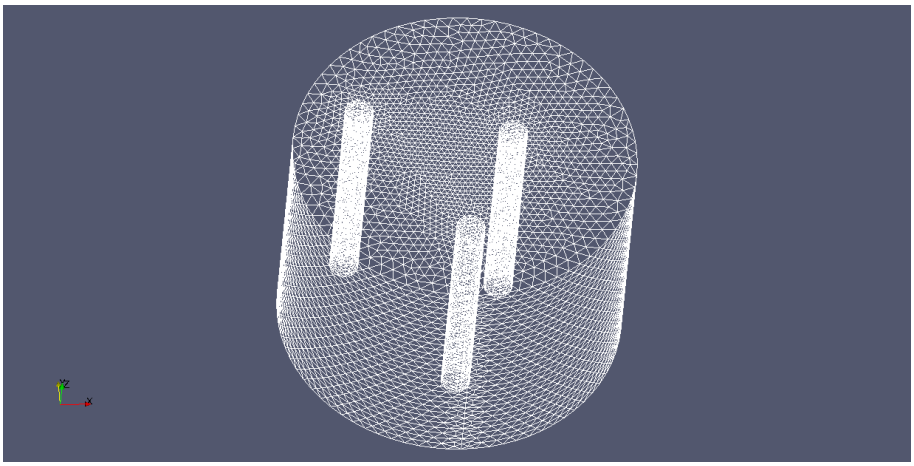

Figure 15: Spatial mesh adopted for the three rods model.

- within fuel domain

$$
\begin{aligned}
m_{\text{fuel}}(u,v;\mu) &= \int_{\Omega_{\text{fuel}}} \left[\frac{1}{\mathrm{v}_1^f} \Phi_1 \psi_{\Phi_1} + \frac{1}{\mathrm{v}_2^f} \Phi_2 \psi_{\Phi_2} + \sum_{i=1}^{8} c_i \psi_{c_i} \right], \qquad (5.1) \\
a_{\text{fuel}}(u,v;\mu) &= \int_{\Omega_{\text{fuel}}} D_1^f \nabla \Phi_1 \cdot \nabla \psi_{\Phi_1} + \int_{\Omega_{\text{fuel}}} D_2^f \nabla \Phi_2 \cdot \nabla \psi_{\Phi_2} \\
&\quad + \int_{\Omega_{\text{fuel}}} \left[\Sigma_{a_1}^f + \Sigma_{s_{1\to 2}}^f - (1-\beta)\nu\Sigma_{f_1} \right] \Phi_1 \psi_{\Phi_1} \\
&\quad - \int_{\Omega_{\text{fuel}}} \left[\Sigma_{s_{2\to 1}}^f + (1-\beta)\nu\Sigma_{f_2} \right] \Phi_2 \psi_{\Phi_1} \\
&\quad - \int_{\Omega_{\text{fuel}}} \sum_{i=1}^{8} \lambda_i c_i \psi_{\Phi_1} - \int_{\Omega_{\text{fuel}}} \Sigma_{s_{1\to 2}}^f \Phi_1 \psi_{\Phi_2} \\
&\quad + \int_{\Omega_{\text{fuel}}} \left[\Sigma_{a_2}^f + \Sigma_{s_{2\to 1}}^f \right] \Phi_2 \psi_{\Phi_2} - \int_{\Omega_{\text{fuel}}} \sum_{i=1}^{8} \beta_i \nu\Sigma_{f_1} \Phi_1 \psi_{c_i} \\
&\quad - \int_{\Omega_{\text{fuel}}} \sum_{i=1}^{8} \beta_i \nu\Sigma_{f_2} \Phi_2 \psi_{c_i} + \int_{\Omega_{\text{fuel}}} \sum_{i=1}^{8} \lambda_i c_i \psi_{c_i}, \qquad (5.2)
\end{aligned}
$$

- within each subdomain of the control rods

$$
\begin{aligned}
m_l &= \mu_l m_r + (1-\mu_l) m_w, \quad \mu_l = 0 \text{ or } 1, \qquad (5.3) \\
a_l &= \mu_l a_r + (1-\mu_l) a_w, \quad \mu_l = 0 \text{ or } 1, \qquad (5.4)
\end{aligned}
$$

where

$$
m_r(u,v;\mu) = \int_{\Omega} \left[\frac{1}{\mathrm{v}_1^r} \Phi_1 \psi_{\Phi_1} + \frac{1}{\mathrm{v}_2^r} \Phi_2 \psi_{\Phi_2} + \sum_{i=1}^{8} c_i \psi_{c_i} \right], \qquad (5.5)
$$

$$m_w(u,v;\mu) = \int_\Omega \left[\frac{1}{\mathrm{v}_1^w}\Phi_1\psi_{\Phi_1} + \frac{1}{\mathrm{v}_2^w}\Phi_2\psi_{\Phi_2} + \sum_{i=1}^{8} c_i\psi_{c_i} \right], \tag{5.6}$$

$$\begin{aligned} a_r(u,v;\mu) = & \int_\Omega D_1^r \nabla\Phi_1\cdot\nabla\psi_{\Phi_1} + \int_\Omega D_2^r \nabla\Phi_2\cdot\nabla\psi_{\Phi_2} \\ & + \int_\Omega \left[\Sigma_{a_1}^r + \Sigma_{s_{1\to2}}^r - (1-\beta)\nu\Sigma_{f_1}\right]\Phi_1\psi_{\Phi_1} \\ & - \int_\Omega \left[\Sigma_{s_{2\to1}}^r + (1-\beta)\nu\Sigma_{f_2}\right]\Phi_2\psi_{\Phi_1} \\ & - \int_\Omega \sum_{i=1}^{8}\lambda_i c_i\psi_{\Phi_1} - \int_\Omega \Sigma_{s_{1\to2}}^r \Phi_1\psi_{\Phi_2} \\ & + \int_\Omega \left[\Sigma_{a_2}^r + \Sigma_{s_{2\to1}}^r\right]\Phi_2\psi_{\Phi_2} - \int_\Omega \sum_{i=1}^{8}\beta_i\nu\Sigma_{f_1}\Phi_1\psi_{c_i} \\ & - \int_\Omega \sum_{i=1}^{8}\beta_i\nu\Sigma_{f_2}\Phi_2\psi_{c_i} + \int_\Omega \sum_{i=1}^{8}\lambda_i c_i\psi_{c_i}, \end{aligned} \tag{5.7}$$

$$\begin{aligned} a_w(u,v;\mu) = & \int_\Omega D_1^w \nabla\Phi_1\cdot\nabla\psi_{\Phi_1} + \int_\Omega D_2^w \nabla\Phi_2\cdot\nabla\psi_{\Phi_2} \\ & + \int_\Omega \left[\Sigma_{a_1}^w + \Sigma_{s_{1\to2}}^w - (1-\beta)\nu\Sigma_{f_1}\right]\Phi_1\psi_{\Phi_1} \\ & - \int_\Omega \left[\Sigma_{s_{2\to1}}^w + (1-\beta)\nu\Sigma_{f_2}\right]\Phi_2\psi_{\Phi_1} \\ & - \int_\Omega \sum_{i=1}^{8}\lambda_i c_i\psi_{\Phi_1} - \int_\Omega \Sigma_{s_{1\to2}}^w \Phi_1\psi_{\Phi_2} \\ & + \int_\Omega \left[\Sigma_{a_2}^w + \Sigma_{s_{2\to1}}^w\right]\Phi_2\psi_{\Phi_2} - \int_\Omega \sum_{i=1}^{8}\beta_i\nu\Sigma_{f_1}\Phi_1\psi_{c_i} \\ & - \int_\Omega \sum_{i=1}^{8}\beta_i\nu\Sigma_{f_2}\Phi_2\psi_{c_i} + \int_\Omega \sum_{i=1}^{8}\lambda_i c_i\psi_{c_i}. \end{aligned} \tag{5.8}$$

Therefore, according to the affine expansion (3.10) and (3.11), $Q_a = Q_m = 32$.

5.1 Some representative results

In this Section, the main results obtained both during the Offline and Online phases are presented.

5.1.1 Offline phase

During this phase, the RB space is built, the ROM is obtained by projecting the "truth" model on it, and the *a posteriori* error estimation is provided as well. Figure 16 shows the

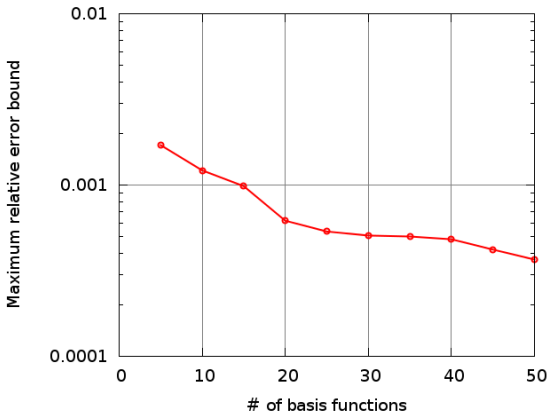

Figure 16: Non-dimensional maximum relative error bound, with respect to the number of basis functions employed. (Minimum $N = 5$).

maximum relative error bound with respect to the number of basis functions employed. The values of the parameters for each point in the graph is chosen according to a POD-greedy algorithm [11, 24]. The whole Offline step lasted almost 200 hours of cpu time. The great increase of the Offline duration, with respect to the approach proposed in the previous Section, is due to the higher number of Q_a and Q_m. Almost the 60% of the time is spent to compute the terms needed by the *a posteriori* error estimation (see Section 3.2.4).

5.1.2 Online phase

During the Online step, the thermal flux has been reconstructed for different combinations of parameters employing 50 basis functions. In the following, the thermal flux is presented within the region of the control rods, on the planes reported in Fig. 17, without displaying the flux within the fuel region for the sake of clarity. In particular, the outcomes provided by the developed ROM are reported in Fig. 18. On the other hand, the solutions assumed as "truth" are depicted in Fig. 19. As it can be seen, the spatial effects induced by the movement of the control rods are accurately reproduced by the reduced model.

Comparing cpu times required to solve the "truth" finite element problem and the developed ROM, reported in Tab. 5, the computational speed-up is of ~ 2000 times per single time step per single cpu. The lower speed-up, with respect to the model developed in the previous Section, is due to the higher number of bilinear forms required by the affine decomposition.

The ratio between the L^2 norms of the error and the solution, for the cases considered, provided by the developed ROM and computed as described in Section 3.2.4, are reported in Tab. 6. Finally, in order to verify the efficiency and rigour of the error bounds, the average, maximum and minimum effectivity (i.e., the ratio between the error bound and the true error between the reduced solution and the high order one) are reported

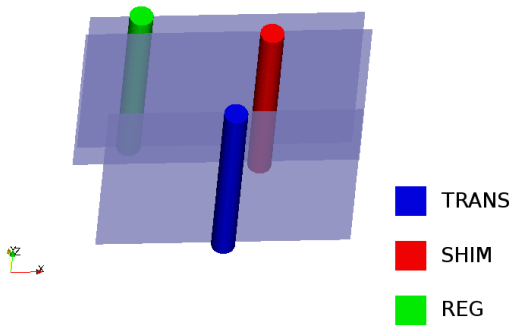

Figure 17: Adopted sections for the visualization of the thermal flux.

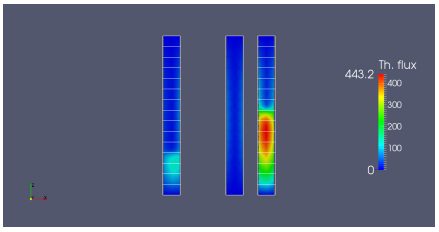

(a) TRANS is inserted, the height of the REG and SHIM is 4 and 8 "steps", respectively

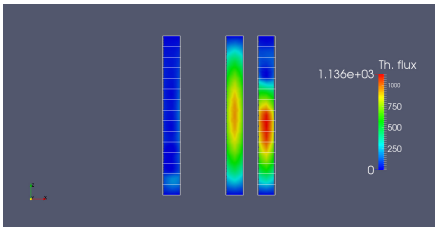

(b) TRANS is withdrawn, the height of the REG and SHIM is 2 and 10 "steps", respectively

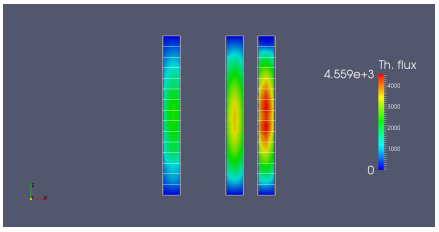

(c) TRANS is withdrawn, the height of the REG and SHIM is 16 and 16 "steps", respectively

Figure 18: Thermal flux $[1/\mathrm{cm}^2\mathrm{s}]$, provided by ROM, inside the control rod spatial domains for different combination of the parameters.

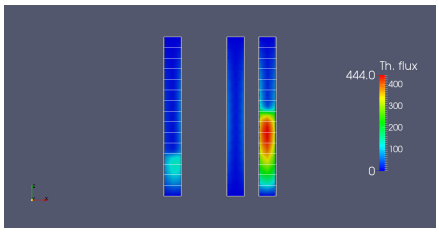

(a) TRANS is inserted, the height of the REG and SHIM is 4 and 8 "steps", respectively

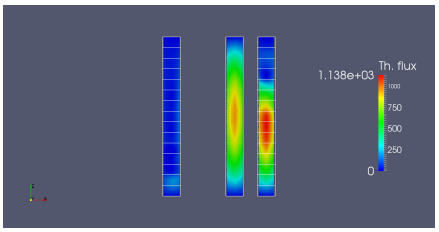

(b) TRANS is withdrawn, the height of the REG and SHIM is 2 and 10 "steps", respectively

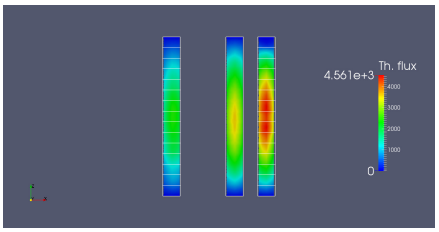

(c) TRANS is withdrawn, the height of the REG and SHIM is 16 and 16 "steps", respectively

Figure 19: Thermal flux $[1/\text{cm}^2\text{s}]$, assumed as "truth" solution, inside the control rod spatial domains for different combination of the parameters.

Table 5: Computational time per single cpu per single time step.

$\mu = \{\text{TRANS, REG, SHIM}\}$	Truth	ROM	Speed-up
$\mu = \{0,4,8\}$	191.0 s	110 ms	1736
$\mu = \{1,2,10\}$	190.4 s	110 ms	1730
$\mu = \{1,16,16\}$	191.1 s	112 ms	1705

Table 6: Relative error bounds in L^2 norm, at the last time step.

$\mu = \{\text{TRANS, REG, SHIM}\}$	Error bounds
$\mu = \{0,4,8\}$	6.02×10^{-5}
$\mu = \{1,2,10\}$	1.92×10^{-4}
$\mu = \{1,16,16\}$	1.14×10^{-4}

in Tab. 7. Such values have been computed for 100 different instances, randomly chosen, of the parameters and for different mesh size in order to investigate the influence of the mesh size on the effectivity and they are in agreement with general considerations in [26, 30].

Table 7: Effectivity.

Mesh size	Average	Maximum	Minimum
h=6 mm	5.255	11.086	1.442
h/2	6.217	12.979	1.430
2h	28.542	60.395	8.550

The break-even (see Eq (4.4)) for this case is given by

$$\text{break-even} = \frac{\sim 200\,\text{h}}{\sim 10\,\text{min}} = 1200. \tag{5.9}$$

Therefore, if more than 1200 full-order simulations have to be computed, the reduced order model should be preferred.

6 Conclusions and perspectives to multi-physics

In this work, two different approaches for simulating the movement of nuclear reactor control rods, in a 3D framework, have been proposed. In order to provide the outcomes in a rapid and reliable way, the certified Reduced Basis method has been employed. The neutronic behaviour has been modelled according to the so-called multi-group diffusion equation [5], which is, in fact, a set of coupled (parametrized) parabolic equations (ten in our problem). The heights of the rods (i.e., how much the rods are withdrawn) are the varying parameters, which are geometric-type parameters. The parametrized bilinear form associated to the elliptic part of the system is non-symmetric and non-coercive, yet it can be affinely decomposed.

As far as the first approach is considered, the movement of a single control rod has been modelled. In particular, a piece-wise affine transformation based on subdomain division has been developed, where the subdomain shapes change in order to simulate the movement of the rod. On the other hand, in the second approach, all the three control rods of the TRIGA Mark II nuclear reactor of the University of Pavia (Italy) have been

taken into account. In order to present a different methodology, the movement of the rods has been discretized like a staircase.

Both the reduced models are capable to accurately reproduce the neutron flux distribution allowing to take into account the spatial effects induced by the control rods, whose height can be set in the Online phase. Moreover, the computational time required to solve the reduced system is four (three) order of magnitude lower with respect to the fine finite element discretization, for the first (second) approach, respectively. The lower speed-up provided by the second approach is due to the higher number of the terms of the affine expansion.

It is worth mentioning that the presented methodology is general and it could also be employed for other industrial relevant problems with 3D parametrized time-dependent models to be considered.

This contribution is thought to be useful for real-time control-oriented studies in the nuclear engineering field, and might be a first step towards a higher-fidelity multi-physics reduced order model of the real reactor considered. To this aim, a detailed core geometry (e.g., without homogenizing the fuel pins) will be employed in future developments. In order to extend the presented approach to a multi-physics parametrized system several challenges have to been addressed. Neutronics and thermal-hydraulics are coupled in a non-linear fashion due to the Doppler effects, as well has thermal-expansion effects. Therefore, suitable strategies for handling such non-linearities have to be developed. Moreover, neutronics and thermal-driven phenomena feature response time that differs of some orders of magnitude and a proper time integration technique should be considered. A reduced order model of a multi-physics parametrized problem, where the neutronics and the thermal-hydraulics are coupled in time-invariant settings is ongoing [33].

A Geometrical parametrization: a 3D example

In this Appendix, we show how the affine transformation (3.15) can be defined for a parametrized tetrahedron, which is the most elementary building block for a 3D geometry. More details can be found in [6]. Let the two tetrahedra shown in Fig. 20 be considered. The reference domain is $\mu-$independent, while the desired, or original, domain is $\mu-$dependent. In order to derive the translation vector $C : \mathcal{D} \to \mathbb{R}^3$ and linear transformation matrix $G : \mathcal{D} \to \mathbb{R}^{3\times 3}$ let the following matrix $\mathbb{B} \in \mathbb{R}^{12\times 12}$ and vector $\mathbb{V}(\mu)$ be

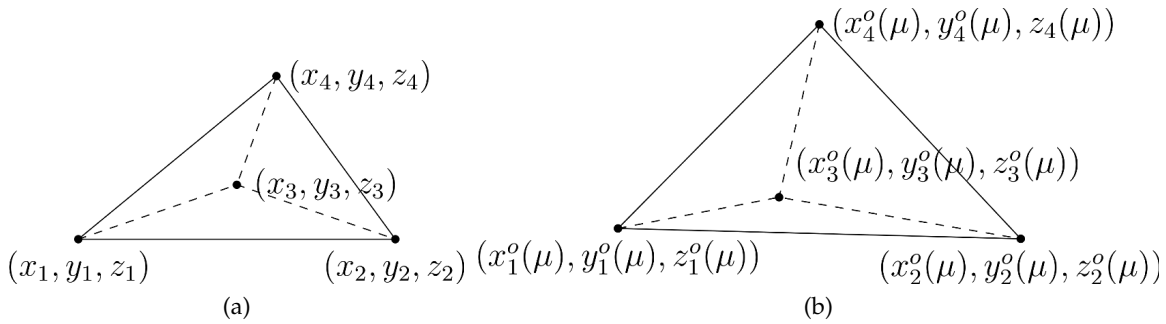

Figure 20: (a) Reference domain Ω, and (b) Original domain $\Omega(\mu)$.

defined,

$$\mathbb{B} = \begin{bmatrix} 1 & 0 & 0 & x_1 & y_1 & z_1 & 0 & 0 & 0 & 0 & 0 & 0 \\ 0 & 1 & 0 & 0 & 0 & 0 & x_1 & y_1 & z_1 & 0 & 0 & 0 \\ 0 & 0 & 1 & 0 & 0 & 0 & 0 & 0 & 0 & x_1 & y_1 & z_1 \\ 1 & 0 & 0 & x_2 & y_2 & z_2 & 0 & 0 & 0 & 0 & 0 & 0 \\ 0 & 1 & 0 & 0 & 0 & 0 & x_2 & y_2 & z_2 & 0 & 0 & 0 \\ 0 & 0 & 1 & 0 & 0 & 0 & 0 & 0 & 0 & x_2 & y_2 & z_2 \\ 1 & 0 & 0 & x_3 & y_3 & z_3 & 0 & 0 & 0 & 0 & 0 & 0 \\ 0 & 1 & 0 & 0 & 0 & 0 & x_3 & y_3 & z_3 & 0 & 0 & 0 \\ 0 & 0 & 1 & 0 & 0 & 0 & 0 & 0 & 0 & x_3 & y_3 & z_3 \\ 1 & 0 & 0 & x_4 & y_4 & z_4 & 0 & 0 & 0 & 0 & 0 & 0 \\ 0 & 1 & 0 & 0 & 0 & 0 & x_4 & y_4 & z_4 & 0 & 0 & 0 \\ 0 & 0 & 1 & 0 & 0 & 0 & 0 & 0 & 0 & x_4 & y_4 & z_4 \end{bmatrix}, \quad \mathbb{V}(\mu) = \begin{bmatrix} x_1^o(\mu) \\ y_1^o(\mu) \\ z_1^o(\mu) \\ x_2^o(\mu) \\ y_2^o(\mu) \\ z_2^o(\mu) \\ x_3^o(\mu) \\ y_3^o(\mu) \\ z_3^o(\mu) \\ x_4^o(\mu) \\ y_4^o(\mu) \\ z_4^o(\mu) \end{bmatrix}, \tag{A.1}$$

where $\mathbb{V}(\mu)$ is the vector of coordinates of nodes of the original domain. Then, the translation vector $C : \mathcal{D} \to \mathbb{R}^3$ and linear transformation matrix $G : \mathcal{D} \to \mathbb{R}^{3\times 3}$ can be obtained as follows:

$$\begin{aligned}[C_1(\mu), C_2(\mu), C_3(\mu), G_{11}(\mu), G_{12}(\mu), G_{13}(\mu), G_{21}(\mu), G_{22}(\mu), G_{23}(\mu),\\ G_{31}(\mu), G_{32}(\mu), G_{33}(\mu)]^T = \mathbb{B}^{-1}\mathbb{V}(\mu).\end{aligned} \tag{A.2}$$

It is worth mentioning that $\mathbb{B}$ is non-singular as long as the four points on the reference domain do not belong to the same plane. Therefore, the affine transformation (3.15), for the problem addressed in this work, can be computed choosing four points, among the vertices of the subdomain, which do not belong to the same plane.

Acknowledgments

We acknowledge CINECA and Regione Lombardia LISA computational initiative, for the availability of high performance computing resources and support. G. Rozza acknowledges INDAM-GNCS national activity group and NOFYSAS program of SISSA.

References

[1] M. Barrault, Y. Maday, N. C. Nguyen, and A. T. Patera. An 'empirical interpolation' method: application to efficient reduced-basis discretization of partial differential equations. *Comptes Rendus Mathematique*, 339(9):667–672, 2004.

[2] G. Bell and S. Glasstone. *Nuclear reactor theory*. Van Nostrand Reinhold Co., 1970.

[3] A. Chatterjee. An introduction to the proper orthogonal decomposition. *Current Science*, 78:808–817, 2000.

[4] R. Dautray and J. L. Lions. *Mathematical Analysis and Numerical Methods for Science and Technology: Volume 6 Evolution Problems II*. Springer-Verlag Berlin Heidelberg, 2000.

[5] J. J. Duderstadt and L. J. Hamilton. *Nuclear Reactor Analysis*. John Wiley and Sons, New York, 1976.

[6] F. Gelsomino and G. Rozza. Comparison and combination of reduced-order modelling techniques in 3D parametrized heat transfer problems. *Mathematical and Computer Modelling of Dynamical Systems*, 17(4):371–394, 2011.

[7] General Atomic Company, U.S.A. *TRIGA Mark II Reactor General Specifications and Description*, 1964.

[8] C. Geuzaine and J. F. Remacle. Gmsh: A 3-D finite element mesh generator with built-in pre-and post-processing facilities. *International Journal for Numerical Methods in Engineering*, 79(11):1309–1331, 2009.

[9] GIF. A Technology Roadmap for Generation IV Nuclear Energy System. Technical report, GIF-002-00, 2002.

[10] M. A. Grepl and A. T. Patera. A posteriori error bounds for reduced-basis approximations of parametrized parabolic partial differential equations. *ESAIM: Mathematical Modelling and Numerical Analysis*, 39:157–181, 1 2005.

[11] B. Haasdonk and M. Ohlberger. Reduced basis method for finite volume approximations of parametrized linear evolution equations. *ESAIM: Mathematical Modelling and Numerical Analysis*, 42(2):277–302, 2008.

[12] P. Holmes, J. Lumley, and G. Berkooz. *Turbolence, Coherent Structures, Dynamical Systems and Symmetry*. Cambridge University Press, 1996.

[13] D. Huynh, D. Knezevic, Y. Chen, J. S. Hesthaven, and A. Patera. A natural-norm successive constraint method for inf-sup lower bounds. *Computer Methods in Applied Mechanics and Engineering*, 199(29):1963–1975, 2010.

[14] D. B. P. Huynh, G. Rozza, S. Sen, and A. T. Patera. A successive constraint linear optimization method for lower bounds of parametric coercivity and inf–sup stability constants. *Comptes Rendus Mathematique*, 345(8):473–478, 2007.

[15] B. S. Kirk, J. W. Peterson, R. H. Stogner, and G. F. Carey. `libMesh`: A C++ Library for Parallel Adaptive Mesh Refinement/Coarsening Simulations. *Engineering with Computers*, 22(3–4):237–254, 2006.

[16] D. J. Knezevic and J. W. Peterson. A high-performance parallel implementation of the certified reduced basis method. *Computer Methods in Applied Mechanics and Engineering*, 200:1455 – 1466, 2011.

[17] A. Koning, R. Forrest, M. Kellett, R. Mills, H. Henriksson, and Y. Rugama. The JEFF-3.1 Nuclear Data Library. Technical Report NEA – OECD, JEFF Report 21, 2006.

[18] K. S. Krane. *Introductory nuclear physics*. Wiley, India, 1987.

[19] J. R. Lamarsh. *Introduction to nuclear reactor theory, 3rd Edition*. Addison-Wesley Publishing Company, 1977.

[20] J. R. Lamarshi and A. J. Baratta. *Introduction to nuclear engineering*. Prentice-Hall, New Jersey, 2001.

[21] T. Lassila, A. Manzoni, and G. Rozza. On the approximation of stability factors for general parametrized partial differential equations with a two-level affine decomposition. *ESAIM: Mathematical Modelling and Numerical Analysis*, 46(6):1555–1576, 2012.

[22] Y. Maday. Reduced basis method for the rapid and reliable solution of partial differential equations. In *Proceedings of International Conference of Mathematicians, Madrid. European Mathematical Society Eds.*, 2006.

[23] A. Manzoni, A. Quarteroni, and G. Rozza. Computational Reduction for Parametrized PDEs: Strategies and Applications. *Milan Journal of Mathematics*, 80(2):283–309, 2012.

[24] N. C. Nguyen, G. Rozza, D. B. P. Huynh, and A. T. Patera. Reduced Basis Approximation and a Posteriori Error Estimation for Parametrized Parabolic PDEs: Application to Real-Time Bayesan Parameter Estimation, John Wiley & Sons, Ltd, 2010, Ch. 8, 157–185.

[25] N. C. Nguyen, G. Rozza, and A. T. Patera. Reduced basis approximation and a posteriori error estimation for the time-dependent viscous Burgers' equation. *Calcolo*, 46(3):157–185, 2009.

[26] A. T. Patera and G. Rozza. Reduced Basis Approximation and A Posteriori Error Estimation for Parametrized Partial Differential Equations, MIT Pappalardo Graduate Monographs in Mechanical Engineering, online at http://augustine.mit.edu, 2007.

[27] A. Quarteroni, G. Rozza, and A. Manzoni. Certified reduced basis approximation for parametrized partial differential equations and applications. *Journal of Mathematics in Industry*, 1(1):1–49, 2011.

[28] A. Quarteroni and A. Valli. *Numerical approximation of partial differential equations. Volume 23*. Springer, 2008.

[29] G. Rozza. Fundamentals of Reduced Basis Method for problems governed by parametrized PDEs and applications. In *CISM Lectures notes "Separated Representation and PGD based model reduction: fundamentals and applications"*. Chinesta, F. and Ladeveze, P. (eds.), Springer Vienna, 2014.

[30] G. Rozza, D. Huynh, and A. Patera. Reduced basis approximation and a posteriori error estimation for affinely parametrized elliptic coercive partial differential equations. *Archives of Computational Methods in Engineering*, 15(3):1–47, 2008.

[31] A. Sartori, D. Baroli, A. Cammi, D. Chiesa, L. Luzzi, R. Ponciroli, E. Previtali, M. E. Ricotti, G. Rozza, and M. Sisti. Comparison of a Modal Method and a Proper Orthogonal Decomposition approach for multi-group time-dependent reactor spatial kinetics. *Annals of Nuclear Energy*, 71:217 – 229, 2014.

[32] A. Sartori, D. Baroli, A. Cammi, L. Luzzi, and G. Rozza. A Reduced Order Model for Multi-Group Time-Dependent Parametrized Reactor Spatial Kinetics. In *Proceedings of the 2014 22nd International Conference on Nuclear Engineering (ICONE22), Prague, Czech Republic, July 7-11, 2014, Paper 30707*, ©ASME 2014.

[33] A. Sartori, A. Cammi, L. Luzzi, and G. Rozza. Multi-physics reduced order models for analysis of Lead Fast Reactor single channel. *Annals of Nuclear Energy*, 2015. In press.
[34] M. A. Schultz. *Nuclear reactor kinetics and control*. McGraw-Hill, 1961.
[35] PSG2 / Serpent Monte Carlo Reactor Physics Burnup Calculation Code, 2011. URL http://montecarlo.vtt.fi.